Phytopathology https://doi.org/10.1094/PHYTO-11-20-0526-R

Accepted: 8 January 2021

Pseudomonas savastanoi pv. *mandevillae* pv. nov., a clonal pathogen causing an emerging, devastating disease of the ornamental plant *Mandevilla* spp.

Eloy Caballo-Ponce[1,2], Adrián Pintado[1,2], Alba Moreno-Pérez[1,2], Jesús Murillo[3], Kornelia Smalla[4], Cayo Ramos[1,2*]

[1]Área de Genética, Facultad de Ciencias, Universidad de Málaga, Campus Teatinos s/n, E-29010 Málaga, Spain.

[2]Instituto de Hortofruticultura Subtropical y Mediterránea “La Mayora”, Consejo Superior de Investigaciones Científicas (IHSM-UMA-CSIC), Málaga, Spain.

[3]Institute for Multidisciplinary Research in Applied Biology, Universidad Pública de Navarra, Mutilva Baja, E-31192, Spain.

[4]Julius Kühn-Institut Federal Research Centre for Cultivated Plants, Institute for Epidemiology and Pathogen Diagnostics, D-38104 Braunschweig

*Correspondence: Cayo Ramos; crr@uma.es

Keywords: *Pseudomonas syringae* complex; *Pseudomonas amygdali*; host range; knot disease; new pathovar; phytohormones; type III secretion system; type III effectors; comparative genomics; phylogenomics; metabolic profile.

Funding: E.C.P, A.M.P, A.P, C.R and J.M were supported by grants FPI/BES-2012-052398, FPI/BES-2015-074847, FPU14/05551, AGL2017-82492-C2-1-R and AGL2017-82492-C2-2-R, respectively, from *Ministerio de Ciencia, Innovación y Universidades* (Spain), cofinanced by the *Fondo Europeo de Desarrollo Regional* (FEDER).

ABSTRACT

Commercial production of the ornamental plant dipladenia (*Mandevilla* spp.) is threatened by dipladenia leaf and stem spot disease, caused by the bacterium *Pseudomonas savastanoi*. *P. savastanoi* includes four pathovars of woody hosts differentiated by a characteristic host range in olive, oleander, ash and broom plants. However, isolates from dipladenia have not been ascribed to any particular lineage or *P. savastanoi* pathovar. Here we report that isolates from dipladenia represent a distinct, clonal lineage. First, dipladenia isolates display very similar plasmid profiles, including a plasmid encoding the *iaaM* gene for biosynthesis of indole-3-acetic acid. Second, multilocus sequence analysis and core-genome single-nucleotide-polymorphisms phylogenies showed a monophyletic origin for dipladenia isolates, which cluster with isolates from oleander (pathovar *nerii*) in a distinct clade well separated from other *P. savastanoi* strains. Metabolic profiling and cross-pathogenicity tests in olive, oleander, ash, broom and dipladenia clearly distinguished dipladenia isolates from the four *P. savastanoi* pathovars. Comparative genomics of the draft genome sequence of the dipladenia strain Ph3 with the other four pathovars showed that Ph3 encodes very few strain-specific genes, and a similar set of virulence genes to pv. *nerii*, including its repertoire of type III secretion system effectors. However, hierarchical clustering based on the catalogue of effectors and their allelic variants clearly separated Ph3 from pv. *nerii* strains. Based on their distinctive pathogenicity profile, we propose a *de novo* pathovar for *P. savastanoi* isolates from dipladenia, *P. savastanoi* pv. *mandevillae* pv. nov., for which strain Ph3 (CFBP 8832^{PT}) has been designated as the pathotype strain.

INTRODUCTION

Dipladenia (*Mandevilla* spp.) encompasses 176 accepted species according to the World Checklist of Selected Plant Families (https://wcsp.science.kew.org), which are evergreen creeper bushes, sometimes reaching up to ten meters high, native to tropical regions from Central and South America. Plants from this genus are highly appreciated for their smooth and intense green leaves, and for their trumpet-shaped flowers in red, pink, white or yellow, held by long stalks. Mostly marketed as herbaceous-looking young plants, mature dipladenias are woody-stemmed vines. Additionally, the flowering period begins in spring and commonly extends until fall, converting dipladenia into a profitable product for the ornamentals market. In fact, the current high commercial demand of dipladenia places this crop in a privileged position among the top ornamental leaders in the new emerging markets (Oder et al. 2016). However, commercial production is severely threatened by dipladenia leaf and stem spot (MaLSS) disease. This emergent disease is caused by the most prevalent bacterial pathogen of dipladenia, *Pseudomonas savastanoi*. The first report of this disease dates back to 2010 in the USA (Putnam et al. 2010), with European outbreaks occurring over the following years in France, Germany (Eltlbany et al. 2012), Slovenia (Pirc et al. 2015) and Spain (Caballo-Ponce and Ramos 2016). With Spain and Italy as the main producers of dipladenia in Europe, this emergent disease has also become a serious concern for European growers. The rapid spread of the pathogen within greenhouses, difficulties for disease management and the visual symptoms of MaLSS are responsible for the loss of a large number of plants, which are classified as unmarketable, as reported for up to 70% of the dipladenia in Slovenian greenhouses (Pirc et al. 2015).

P. savastanoi belongs to *Pseudomonas syringae sensu lato*, a bacterial complex with an unresolved taxonomic status comprising 15 previously defined *Pseudomonas* species associated with plants and the water cycle, and that can

be separated into 13 distinct phylogroups (PG) (Berge et al. 2014; Gomila et al. 2017). The species *P. savastanoi* belongs to phylogroup 3 (PG3), the only phylogroup comprising bacteria that cause tumorous overgrowths (knots) in woody hosts (Lamichhane et al. 2014). In particular, *P. savastanoi* currently comprises four different pathovars of woody hosts, namely *P. savastanoi* pv. *savastanoi* (Psv), *P. savastanoi* pv. *nerii* (Psn), *P. savastanoi* pv. *fraxini* (Psf) and *P. savastanoi* pv. *retacarpa* (Psr), including strains isolated from olive (*Olea europaea*), oleander (*Nerium oleander*), ash (*Fraxinus excelsior*) and broom (*Retama sphaerocarpa*), respectively (Bull et al. 2010; Gardan et al. 1992). These pathovars produce knots (Psv, Psn and Psr) or excrescences (Psf), typically in the trunks, stems and branches of infected plants (Caballo-Ponce et al. 2017a). In turn, *P. savastanoi* infections of dipladenia are characterized by the generation of necrotic spots surrounded by a chlorotic halo on leaves and stems, as well as knot formation on stems (Eltlbany et al. 2012; Caballo-Ponce and Ramos 2016). Besides the diversity of symptoms produced by these pathovars, their hosts are also phylogenetically diverse, belonging to the family Oleaceae (olive, ash, and many other hosts), Apocynaceae (oleander and dipladenia) and Fabaceae (broom), among other plant hosts (Caballo-Ponce et al. 2017a; Morris et al. 2019).

Despite its economic impact, there is a paucity of information on the management of MaLSS, its progress in infected plants and the biology and genetics of *P. savastanoi* strains infecting dipladenia. In particular, the pathogen has not been ascribed to any particular lineage or pathovar within the species *P. savastanoi*. Metabolic profiling of seven *P. savastanoi* isolates from France and Germany initially identified the causal agent of MaLSS as Psn or *P. savastanoi* pv. *glycinea*, a pathogen of soybean (*Glycine max*). On the other hand, BOX-PCR fingerprints and phylogenetic analysis of partial nucleotide sequences of the 16S rRNA gene showed that these seven isolates clustered together with Psn and Psv strains. However, cross-pathogenicity tests performed in olive and

oleander could not confidently classify the isolates as members of any of these two pathovars (Eltlbany et al. 2012). Although partial sequencing of the *rpoD* gene from two Slovenian isolates showed a closer proximity to Psn strains (Pirc et al. 2015), results from pathogenicity tests in oleander plants were not reported. Additionally, hybridization analyses of Southern-blotted plasmid restriction digests with probes generated from plasmid-borne *P. syringae* genes, showed that the profiles obtained from seven dipladenia isolates were highly similar but clearly distinct from those of Psv and Psn strains, which showed high strain-specific variability (Eltlbany et al. 2012). Moreover, and unlike most *P. savastanoi* strains, dipladenia isolates do not trigger a hypersensitive response (HR) in tobacco leaves (Pirc et al. 2015; Caballo-Ponce and Ramos 2016). All these initial observations suggest that *P. savastanoi* strains infecting dipladenia might constitute a separate, homogeneous lineage holding a distinct set of plasmids. This perceived homogeneity contrasts with the variability previously observed for the four *P. savastanoi* pathovars from woody hosts: although they correspond to well-defined genetic lineages, they show a degree of variability in intrapathovar virulence gene repertoires, plasmid profile, virulence, arbitrarily-primed PCR, real-time PCR and high-resolution melting analysis (Pérez-Martínez et al. 2008; Tegli et al. 2010; Gori et al. 2012; Moretti et al. 2017; Moreno-Pérez et al. 2020), among other characteristics. Nevertheless, and because dipladenias are reproduced vegetatively, we cannot discount the possibility that the small number of dipladenia isolates characterized so far belong to a particular clonal lineage that was dispersed with plant material, rather than being representative of their variability as a whole. Therefore, characterization of these isolates deserves attention.

In this work we obtained the draft genome sequence of *P. savastanoi* Ph3 and used it in comparative genomic analyses with *P. savastanoi* strains isolated from olive, oleander, ash and broom. Phylogenetic analysis and metabolic and plasmid profiling, in combination with cross-pathogenicity tests, revealed genomic and

132 phenotypic features differentiating *P. savastanoi* strains isolated from dipladenia
133 from all four well-established *P. savastanoi* pathovars of woody hosts. We
134 propose a new pathovar closely related to Psn, *P. savastanoi* pv. *mandevillae*
135 (Psm) pv. nov., as the causal agent of MaLSS and Psm Ph3 (CFBP 8832^{PT}) as
136 its pathotype strain.

MATERIALS AND METHODS

Bacterial strains, media and growth conditions. Wild-type *P. savastanoi* strains used in this study are listed in Table 1. Psm Ph3 derivatives transformed with plasmids are described below. *P. savastanoi* was grown at 28 °C in lysogeny broth (LB) medium (Bertani 1951), super optimal broth (SOB) (Hanahan 1983) and in King's B (KB) medium (King et al. 1954). When required, media were supplemented with the appropriate antibiotics at the following final concentrations: kanamycin (Km) 10 µg/ml; nitrofurantoin 20 µg/ml; and cycloheximide 100 µg/ml.

Plasmid DNA techniques. Plasmid minipreparations of Psm isolates were made as previously described (Zhou et al. 1990) with some modifications to minimize the isolation of chromosomal DNA (Murillo and Keen 1994). Plasmids were separated by electrophoresis in 0.8 % agarose gels in TAE buffer for 4 hours at 60V, and then stained with ethidium bromide before imaging. A DNA probe from the *iaaM* gene was amplified and labeled by PCR using primers and digoxigenin-dNTPs from the Dig labeling mix kit (Roche Applied Science, Mannheim, Germany) according to the supplier's instructions. Plasmid preparations blotted on nylon membranes were hybridized with the probe at 65 °C as previously described (Pérez-Martínez et al. 2008).

Bioinformatics methods. *Genome sequencing of Psm strain Ph3. P. savastanoi* Ph3 was grown overnight at 28 ºC in LB broth, bacteria were then collected by centrifugation and genomic DNA was purified using the JetFlex Genomic DNA Purification Kit (Genomed, Löhne, Germany) according to the manufacturer's guidelines. The resulting DNA sample was purified by two subsequent extractions with 25:24:1 phenol-chloroform-isoamyl alcohol and 24:1 chloroform:isoamyl alcohol (volumetric proportions), precipitated with 100 % ethanol and 3 M sodium acetate pH 5.2 and resuspended in bi-distilled water. The purity and concentration of genomic DNA were measured

spectrophotometrically. DNA was sequenced at the Center for Biomedical Research of La Rioja (CIBIR, Spain) using Illumina Genome Analyzer IIx. The sequencing yielded over 22.5 million reads (coverage, 250x) that were imported as a pair-end file and assembled with CLC Genomics Workbench v. 7.0.4 with default settings, producing 256 contigs with a total length of 5.87 Mb and an average GC content of 58.1 %. The genome was automatically annotated upon submission to GenBank (accession no. NIAX00000000) at National Centre for Biotechnology Information (NCBI).

Phylogenetic analyses. Phylogenetic relationships were predicted by multilocus sequence analysis (MLSA) using partial sequences of the g*yrB*, *rpoD*, *gapA*, *rpoA* and *recA* genes. Sequences corresponding to Psv, Psn, Psf and Psr strains were downloaded from GenBank. For Psm isolates, partial sequences were generated following PCR amplification with GoTaq Flexi DNA polymerase (Promega, Madison, WI, USA) and the primers listed in Table S1. Sequencing was performed by STAB VIDA, Lda. (Caparica, Portugal). A maximum likelihood phylogeny based on the concatenated sequence of these five genes (total length 3219 nt), using the Tamura-Nei model and with 100 bootstraps replicates, was constructed using MEGA7 (Kumar et al. 2016). The *P. savastanoi* phylogeny was also analyzed using core genome single nucleotide polymorphisms (SNPs) with the programs Parsnp v1.2 and Gingr v1.2 (Treangen et al. 2014), and 100 bootstrap replicates; trees were visualized and manipulated using MEGA 7 (Kumar et al. 2016).

Comparative genomic analyses. The core genome analyses were performed using the Bacterial Pan Genome Analysis (BPGA) tool BPGA v1.3 (Chaudhari et al. 2016) with assemblies downloaded from the NCBI. Using the USEARCH algorithm (Edgar 2010) within BPGA, and with a threshold of 0.9 (90 % BLASTP identity), we identified orthologous genes, strain-specific genes and genes encoded in two to four genomes (accessory genes). The list of strain-specific genes was annotated using BLASTP and Sma3s.v2 software (Casimiro-Soriguer

et al. 2017) and then manually classified into functional categories according to the predicted functions of their annotated products. Virulence gene repertoires were predicted using PIFAR, a tool for the identification of plant-bacteria interaction factors in bacterial genomes (Martínez-García et al. 2016). Average nucleotide identity (ANI) was calculated with the orthologous ANI algorithm using BLASTN, implemented in the standalone program OAT (https://www.ezbiocloud.net/tools/orthoani) (Lee et al. 2016).

Prediction of T3SS and its effectors. Structural and regulatory components of the type III secretion system (T3SS) were identified using the web-based tool T346 Hunter (Martínez-García et al. 2015). Prediction of T3SS effectors (T3Es) was made using PIFAR (Martínez-García et al. 2016), which searches for T3Es homologs on three other platforms, namely, The *Pseudomonas syringae* Genome Resources (http://www.pseudomonas-syringae.org/), Ralsto T3E (Peeters et al. 2013) and The *Xanthomonas* Resource (http://www.xanthomonas.org/). The identified T3Es sequences were manually examined for truncations, disruptions and frameshifts using the bioinformatics software platform Geneious 8.1.9 (Kearse et al. 2012) and the genome browser Artemis 16.0.0 (Carver et al. 2012). Hierarchical clustering of *P. savastanoi* strains based on their T3E content was performed using Morpheus as previously reported (Moreno-Pérez et al. 2020).

Metabolic profiling of *P. savastanoi*. The transformation of 95 compounds by *P. savastanoi* strains was examined with Biolog GN2 microplates (Biolog, Inc., Hayward, CA, USA). Bacteria were incubated on LB plates at 28 ºC for two days, collected and resuspended in 0.4% NaCl to an OD_{590} of 0.2. After loading the plate with these bacterial suspensions (150 µl/well), plates were incubated at 28 ºC in an orbital shaker at 150 rpm and monitored for one week. When the substrates are oxidized by the strains, a purple dye develops visible patterns of positive (deep purple) and negative (clear) wells. Partial oxidation (light purple) was taken as a weak positive (w). Hierarchical clustering of *P. savastanoi* strains

based on their metabolic profiles was performed with a presence-absence matrix with values of “0” (-), “1” (w) and “2” (+). To measure the distance between strains, the similarity matrix was made with the Euclidean distance method using Morpheus software (https://software.broadinstitute.org/morpheus/). Then, the tree was constructed by the neighbor-joining method using MEGA7 (Kumar et al. 2016).

Plant infections. Bacterial suspensions in 10 mM $MgCl_2$ containing approximately 10^8 colony forming units (cfu)/ml were infiltrated into the abaxial side of *Nicotiana tabacum* cv. Xanthi leaves using a needle-less syringe, to test for HR elicitation. Symptoms were recorded 48 hours post-infiltration with a high-resolution camera (Canon D6200, Canon Corporation, Tokyo, Japan). Psm strains do not induce the HR on tobacco plants, but it is not known whether their T3Es are not recognized or if this is due to a non-functional T3SS in this host. To differentiate between these alternatives, we decided to evaluate the HR-inducing activity of a Psm strain ectopically expressing a T3E known to induce the HR on tobacco. Then, plasmid pAME8 (Macho et al. 2009), a pBBR1-MCS4 derivative encoding a transcriptional fusion of *avrRpt2* from *P. syringae* pv. *tomato* strain 1065 to the *nptII* and *lacZ* promoters, was transformed into Psm Ph3 cells by electroporation as previously described (Pérez-Martínez et al. 2007). Transformants were selected on LB agar plates containing Km and single colonies were verified by PCR. One of the transformants (Ph3-AvrRpt2) was selected to test elicitation of the hypersensitive response (HR) in *N. tabacum* cv. Xanthi leaves as described above.

Plant material was sanitized with 300 g/hl of Bordeaux mixture (20% $CuSO_4$) and, after 3 weeks, was washed with 70% ethanol and air dried prior to inoculation. Dipladenia plants (*Mandevilla* spp.) var. pink flowers, *O. europaea* plants derived from a seed germinated *in vitro* (originally collected from an “Arbequina” plant), *N. oleander* plants accession “white” supplied by Viveros Guzmán (Málaga, Spain), and *F. excelsior* and *R. sphaerocarpa* plants native

from Valladolid and supplied by Viveros Fuenteamarga (Valladolid, Spain) were wounded along the stem with a scalpel, and approximately 10^6 cfu were placed per wound. For broom plants, around 10^7 cfu/wound were inoculated using a needle coupled to a syringe. After inoculation, wounds were wrapped with parafilm (Bemis, Neenah, WI, USA) for 7 days. Three dipladenia plants and two plants of the other hosts per strain were inoculated as previously described (Penyalver et al. 2006; Moreno-Pérez et al. 2020). The number of wound sites infected per plant varied between 5 and 10, depending on the size of the plant. Plants were kept in a greenhouse for three months under natural photoperiod (15 hours light/9 hours dark) at room temperature (approximately 26 °C day/18 °C night). The resulting symptoms were captured with a high-resolution camera (Canon D6200, Canon Corporation, Tokyo, Japan) 90 days after inoculation. *P. savastanoi* cells were recovered from dipladenia as follows: Knots developed after infection were excised from the plants and homogenized by mechanical disruption in 10 mM $MgCl_2$ using a mortar and a pestle, and serial dilutions were plated on LB containing nitrofurantoin 20 µg/ml and cycloheximide 100 µg/ml.

To monitor the systemic infection of Psm Ph3 in dipladenia plants, Ph3 was transformed by electroporation with plasmid pLRM1-GFP, constitutively expressing the green fluorescent protein (GFP) from the $P_{A1/04/03}$ promoter (Rodriguez-Moreno et al. 2009). The transformant (Ph3-GFP) was inoculated in dipladenia stems and plants were examined with a stereoscopic fluorescence microscope (Leica MZ FLIII) equipped with a 100 W mercury lamp and a filter set GFP2 (excitation 480/40 nm; extinction 510 nm LP). Images were captured 23 days after infection with a high-resolution digital camera (Nikon DXM 1200).

RESULTS

***P. savastanoi* from dipladenia represent a distinct, clonal lineage highly related to *P. savastanoi* pv. *nerii*.** Isolates causing MaLSS from France and Germany were very similar to each other (Eltlbany et al. 2012), and the same occurred for local pathogen populations from Slovenia (Pirc et al. 2015), and Spain (Caballo-Ponce and Ramos 2016). However, it is not clear if they represent highly similar local populations or are representative of the MaLSS pathogen. To test this, we compared diverse phenotypic and genotypic characteristics of a reference collection comprising a representative isolate from each of the five countries where the disease has been reported (Table 1).

Isolates from dipladenia display highly conserved plasmid profiles. Unlike oleander and olive isolates (Caponero et al. 1995; Pérez-Martínez et al. 2008), seven *P. savastanoi* isolates from dipladenia showed nearly identical patterns after native plasmid digestion with Bst1107I and PstI (Eltlbany et al. 2012). However, these observations were restricted to French and German Psm isolates and the number and sizes of native plasmids could not be determined. We therefore examined the plasmid profiles of the five Psm strains collection.

Psm strains displayed very similar plasmid patterns (Figure 1), with bands of approximately 19, 23, 50, 55 and 73 kb present in all the isolates, with the exception of the 73 kb plasmid missing in Psm 1397. Psm Ph5 also showed two additional plasmid bands of approximately 43 and 82 kb. This high conservation is striking and suggests clonality, although plasmid profiles have been reported to be either highly conserved (Gutiérrez-Barranquero et al. 2013; von Bodman and Shaw 1987) or highly variable (Pérez-Martínez et al. 2008; Sato et al. 1982; Ullrich et al. 1993) within pathovars of the *P. syringae* complex.

The approximately 50 kb plasmid of the five Psm isolates hybridized to an *iaaM*-specific probe in Southern blot analyses (Figure S1), confirming previous data using digested plasmid DNA (Eltlbany et al. 2012). Gene *iaaM* is required

for the biosynthesis of high levels of the phytohormone indoleacetic acid and is essential for the induction of tumors by Psv NCPPB 3335 (Aragón et al. 2014). Our results, therefore, suggest that indoleacetic acid might also be essential for the induction of symptoms by Psm in dipladenia.

MLSA, core-genome SNPs and ANI analyses reveal a close relationship between Psm and Psn strains. To determine their evolutionary relationships, we carried out an MLSA analysis of the Psm reference collection and all sequenced *P. savastanoi* strains from woody hosts using concatenated partial DNA sequences of genes *gyrB*, *rpoD*, *gapA*, *rpoA* and *recA*.

The high conservation of these genes provided little resolution. Nevertheless, all Psm isolates clustered together with a few Psn strains in a distinct clade that was well-separated from the remaining *P. savastanoi* strains (Figure 2). In addition, this tree showed a very similar topology to that obtained using SNPs from a core genome alignment of all sequenced *P. savastanoi* strains (Moreno-Pérez et al. 2020), including the draft genome of Psm Ph3 obtained in this work (see below; Figure S2). ANI is extensively used to measure overall similarity between genomes, with a recommended cut-off of 95-96% ANI to delineate species (Lee et al. 2016). Using the OAT program, the Psm Ph3 genome showed 99.90-99.91% identity with Psn strains *Psn23*, CFBP 5067 and ICMP 16944, and 99.78% to Psn ICMP 13781, whereas identity was lower than 99.83% with the genomes of all other sequenced *P. savastanoi* strains from woody hosts. Taken together, these results suggest a monophyletic origin for the Psm genetic lineage and a closer association with pathovar nerii.

Metabolic profiling distinguish Psm isolates from other P. savastanoi from woody hosts. We carried out a comparative metabolic analysis using Biolog GN2 plates to identify differences in nutrient assimilation across *P. savastanoi* strains isolated from ash, dipladenia, oleander, broom and olive. Results revealed that all 14 strains tested yielded complete and negative oxidation for 22 and 23 compounds, respectively (Figure 3, Table S2). However, the five Psm strains

tested were unable to oxidize 13 compounds that could be partially or completely oxidized by the remaining nine tested strains of pathovars Psv, Psn, Psf and Psr. Most of these compounds were sugars (*e.g.* L-fucose, maltose, L-rhamnose and D-melibiose), but also nucleosides (*e.g.* thymidine and uridine), D-amino acids (*e.g.* D-serine) and small organic acids (*e.g.* D, L-lactic acid). Other compounds differentiating *P. savastanoi* pathovars were L-pyroglutamic acid, transformed by all strains except for Psr CECT 4861, and L-ornithine, exclusively oxidized by Psn strains. In a dendrogram obtained from hierarchical cluster analysis of the metabolic profiles, the five Psm isolates were grouped in a distinct branch that was separated from the remaining *P. savastanoi* strains analyzed, including all Psn strains (Figure 3). Importantly, clustering largely agrees with pathovar assignation, suggesting the metabolic adaptation of these bacteria to their plant hosts.

***P. savastanoi* isolates from dipladenia show a distinctive host range and cause systemic infections.** *Cross-pathogenicity tests. P. savastanoi* pathovars *savastanoi*, *nerii*, *fraxini* and *retacarpa* are differentiated by cross-pathogenicity tests in olive, oleander, ash and Spanish broom (Caballo-Ponce et al. 2017a; Moreno-Pérez et al. 2020; Ramos et al. 2012). We therefore examined the pathogenicity of the Psm reference collection on these hosts in comparison with strains of the other pathovars from woody hosts, to determine their pathovar assignation.

Pathogenicity of representative strains of Psv, Psn, Psf and Psr in olive, oleander, ash and Spanish broom (Figure 4A and Table 2) was consistent with previously published results (Alvarez et al. 1998; Iacobellis et al. 1998; Janse 1982; Janse 1991; Moreno-Pérez et al. 2020; Ramos et al. 2012). Additionally, dipladenia stems did not show any symptoms after inoculation with diverse strains of Psv (NCPPB 3335, CFBP 1670 and PseNe107), Psf (NCPPB 1006, NCPPB 1464 and CFBP 5062) and Psr (CECT 4861) (Figure 4B). However, different Psn strains promoted the generation of different symptoms in dipladenia:

CFBP 5067 and ITM 519 induced the formation of knot-like overgrowths, whereas Psn *Psn23* infections were asymptomatic (Figure 4).

The five Psm isolates displayed comparable pathogenicity patterns that also distinguished them from the other four pathovars, inducing symptoms in dipladenia, olive and ash (Figure 4 and Table 2). On dipladenia stems, as expected, all Psm isolates induced knots, reaching similar *in planta* populations of 10^7 - 10^8 cfu per knot. On olive stems, they also induced knots that were similar to those induced by Psv NCPPB 3335 (Figure 4A). All dipladenia isolates were also pathogenic on ash, inducing knots or a swelling at the point of inoculation. Virulence in ash, however, was strain-dependent: Psm Ph5 was the most virulent strain, inducing nine knots and one swelling-like structure, whereas Psm Ph3 exclusively caused swellings (Table 2). In contrast, none of the dipladenia isolates were pathogenic on either oleander or Spanish broom (Figure 4A, Table 2).

In summary, our results demonstrate a distinctive host range for Psm isolates separating them from the four recognized *P. savastanoi* pathovars of woody hosts. Thus, a *de novo* pathovar is assigned to *P. savastanoi* isolated from dipladenia: *P. savastanoi* pv. *mandevillae* pv. nov.

Psm isolates produce systemic infections in dipladenia, leading to plant death. While assaying the pathogenicity of Psm in dipladenia, we occasionally observed the induction of typical symptoms in plant parts far from the point of inoculation, suggesting that the pathogen might spread systemically. To confirm this hypothesis, Psm Ph3 was transformed with pLRM1-GFP, a plasmid expressing the green fluorescent protein (GFP) from a constitutive promoter (Rodriguez-Moreno et al. 2009). The resulting strain, Ph3-GFP, was inoculated in dipladenia stems. After 23 days, we observed clear disease symptoms in the inoculated points as well as in non-inoculated stems of the infected plants (Figure 5A). Likewise, symptomatic non-infected petioles (Figure 5B) and leaves (Figure 5C) displayed strong GFP fluorescence, whereas no fluorescence was detected in

the petioles (Figure 5D) and leaves (Figure 5E) of a non-infected plant. These results thus demonstrate the movement of the pathogen along the plant, causing a systemic infection. Secondary symptoms were more evident with time (Figure 5F), and 90 days after inoculation, the basal two-thirds of most stems were covered with tumors. Leaves showed a pronounced wilting, retaining their color at first but then turning brown and desiccating; however, the basal leaves remained green and apparently healthy.

Comparative genomics of Psm Ph3 with other *P. savastanoi* pathovars from woody hosts. Comparative genomics between phylogenetically related strains has been frequently used to identify strain/pathovar-specific elements that might contribute to host range definition. We therefore obtained a draft genome sequence of Psm Ph3, which yielded a predicted number of genes (5589) and proteins (5111) similar to those previously reported for other *P. savastanoi* genomes (Moreno-Pérez et al. 2020). To unveil Psm Ph3-specific genetic features, we carried out a comparative genomic analysis with the four Psn genomes available in GenBank (Dillon et al. 2019; Moreno-Pérez et al. 2020; Nowell et al. 2016) using two complementary bioinformatics tools, the bacterial pan-genome analysis (BPGA) tool and PIFAR.

Psm Ph3 contains very few strain-specific genes. The analyses identified a core genome composed of 4084 genes, with 720 to 885 accessory genes (present in 2-4 genomes) and 42 to 697 strain-specific genes (Figure 6). Strain-specific genes were annotated and classified into gene ontology (GO) categories using Sma3s.v2 software. The most abundant category found was DNA binding (> 80 genes), followed by ion binding, oxidoreductase activity and signal transducer activity, composed by 37-42 genes (Figure S3). In addition, the 43 Psm Ph3 strain-specific genes were annotated using BLASTP and manually classified into six main categories. The most abundant category comprises 19 genes encoding hypothetical proteins, followed by DNA replication, recombination, mutation and repair (11 genes) and type IV secretion system

elements (8 genes). Thirty of these strain-specific genes were found in a single contig (NZ_NIAX01000040, 27.7 kb), which mostly encoded typical plasmid proteins (Table 3), suggesting that the majority of the strain-specific genes found in the genome of strain Ph3 are encoded in a plasmid not present in any of the Psn strains examined.

The Psm Ph3 genome contains a similar set of virulence genes to Psn strains. The comparative genomic analysis of Psm Ph3 with four Psn strains using PIFAR revealed the presence of characteristic genes involved in the virulence/pathogenicity of *P. savastanoi*. Among those, strain Ph3 contains genes involved in the metabolism of the phytohormones indole-3-acetic acid (*iaaM, iaaH* and *iaaL*) and cytokinins (*idi* and *ptz*) (Figure S4), which were shown to be necessary for tumor induction by Psv NCPPB 3335 (Aragón et al. 2014; Añorga et al. 2020). In this sense, estimation of IAA production in culture supernatants of all Psm strains included in this analysis using the Salkowski reagent (Gordon and Weber 1951) yielded similar concentrations to those obtained for Psv NCPPB 3335 (data not shown). Other typical pathogenicity/virulence factors of *P. savastanoi* found in the genome of Psm Ph3 were a complete T3SS canonical cluster (T-PAI), an additional T3SS resembling that found in *Rhizobium* species (R-PAI), a complete set of type IV secretion system type A (T4SS-A) genes (*virB1*-*virB11* and *virD4*), incomplete sets of T4SS-B and T4SS-C and two different type VI secretion system (T6SS) clusters (Figure S4). Furthermore, genes coding for enzymes involved in cyclic-di-GMP metabolism (BifA and DgcP) and AHL quorum sensing elements (PssI and PssR), as well as the WHOP region, involved in the catabolism of phenolics and exclusively found in *P. syringae* and *P. savastanoi* pathovars of woody hosts (Caballo-Ponce et al. 2017b), were also found.

The Psm Ph3 type III secretion system effector repertoire is highly similar but not identical to that of Psn strains. A previous comparative genomics analysis showed that the *P. savastanoi* pathovars from woody hosts contained variable

T3E repertoires, but that they correlated closely with pathogenic specialization (Moreno-Pérez et al. 2020). The T3E pool of Psm Ph3, determined here using PIFAR (Martínez-García et al. 2016), consisted of 20 complete effectors and eight truncated proteins (HopAS1, AvrPto1, HopAO1, HopAZ1, HopAA1, HopA2, HopM1 and HopW1). Taking into account the phylogenetic proximity between Psm and Psn strains (Figure 2, Figure S2), it was particularly interesting to compare their T3E repertoires. The analysis determined a core of 28 T3Es, highlighting the very close relationship between Psm and Psn strains (Figure 7). This Psn-Psm core includes the 24 T3Es included in the soft-core genome (≥ 95% of the strains) of the four previously established *P. savastanoi* pathovars of woody hosts (Moreno-Pérez et al. 2020), plus HopG1, HopBM1, AvrRpm2 and a novel putative T3E (WP_032074452) recently identified in all *P. savastanoi* strains sequenced (Moreno-Pérez et al. 2020). Notably, Psm Ph3 and all four Psn strains encode specific truncations of AvrPto1 and HopA2*,* as well as a complete version of HopAT1 not found in any of the other three *P. savastanoi* pathovars*.* However, a truncated version of HopAS1 was exclusively found in the Psm Ph3 genome. Furthermore, all Psn strains contain two specific T3E, HopBD1 and HopAF1-1, the latter being absent in strain *Psn23*. In addition to these, HopAY1 is present in Psm Ph3 and all Psn strains except for *Psn23* (Figure 7).

Despite the phylogenetic proximity between Psn and Psm strains (Figure 2, Figure S2) and their highly similar T3E content, hierarchical clustering based on T3E content, including the observed strain-specific T3E truncations, clearly separated Psm Ph3 from the four Psn strains (Figure 7), suggesting that Psm Ph3 encodes exclusive versions of several T3Es that might contribute to define the pathogenicity profile of Psm strains.

Heterologous expression of AvrRpt2 restore HR elicitation to Psm Ph3 in tobacco plants. Strains of *P. syringae sensu lato* are characterized by their ability to induce the hypersensitive response (HR) in tobacco plants, which is dependent on the translocation into plant cells of T3Es recognized by plant resistance (R)

proteins and is a key test in the LOPAT scheme for diagnosis of fluorescent pseudomonads (Hueck 1998; Lelliott et al. 1966). Additionally, the T3SS plays a key role in *P. savastanoi*-host plant interactions (Caballo-Ponce et al. 2017a). However, Slovenian (Pirc et al. 2015) and Spanish (Caballo-Ponce and Ramos 2016) Psm isolates induce the HR on tomato but not on tobacco, suggesting that their specific T3E repertories are recognized in tomato but not in tobacco plants. Psm Ph3 (France), Ph5 (Germany) and 1397 (USA) (Table 1), did not trigger an HR on *N. tabacum* cv. Xanthi leaves (not shown). To test whether heterologous expression in Psm of an HR-inducing T3E in tobacco restored the ability of the strain to elicit the HR in this host, Psm strain Ph3-AvrRpt2, expressing the *avrRpt2* gene from *P. syringae* pv. *tomato* 1065, was infiltrated in tobacco leaves. Gene *avrRpt2* is known to elicit a visible HR in *N. tabacum* cv. Xanthi (Mudgett and Staskawicz 1999) and, thus, necrosis of the inoculated tissue typical of HR was observed in tobacco leaves infiltrated with Psm Ph3 expressing *avrRpt2* while no visible HR was triggered by the wild type strain (Figure 8). Therefore, the inability of Psm Ph3 to induce the HR in tobacco is likely due to a differential T3E repertoire compared to other strains of *P. syringae sensu lato.*

DISCUSSION

In this work, we undertook the characterization and comparative analysis of representative strains isolated from dipladenia in the five countries where MaLSS has been reported (Table 1). Our combination of cross-pathogenicity tests, metabolic and plasmid profiling, and phylogenetic analyzes, combined with comparative genomic analyses of Psm Ph3 with other *P. savastanoi* strains, allowed us to identify a homogeneous group of *P. savastanoi* strains clearly differentiated from those included in the four established *P. savastanoi* pathovars of woody hosts. Based on the unique capabilities of these strains, we propose that the causal agent of MaLSS be identified as a new pathovar of *P. savastanoi* with the name *P. savastanoi* pv. *mandevillae* pv. nov., and strain Ph3 (CFBP 8832^{PT}), whose draft genome sequence is reported here, be designated as the pathotype strain. Following the international standards for naming pathovars of phytopathogenic bacteria (Dye et al. 1980), Psm strains Ph3, Ph5 and MSI13L (Table 1) were included in a permanent collection, the *Collection Francaise de Bacteries Phytopathogenes* (CFBP). Two additional Psm strains, Ph8 (CFBP 8834) and MSI14S (CFBP 8836), isolated in France (Eltlbany et al. 2012) and Spain (Caballo-Ponce and Ramos, 2016), respectively, were also included in this collection.

Psm isolates from France and Germany showed similarity in their patterns of restriction digestion of plasmid DNA as well as their corresponding patterns of Southern hybridization with *iaaM* and *iaaL* probes (Eltlbany et al. 2012). Here we further show that the native plasmid profile is highly conserved among representative Psm strains from all countries where MaLSS has been reported, with all of them containing a native plasmid encoding the *iaaM* gene (Figure 1, Figure S1). In addition, we found a contig (NZ_NIAX01000110, approximately 7.7 Kb) in the Ph3 draft genome encoding the *iaaMH* operon, the *iaaL* and *matE* genes, which are involved in the biosynthesis and transport of IAA-Lys in Psn

(Tegli et al. 2020). This contig shows conserved synteny with the genomes of most Psv, Psn and Psr strains and is likely plasmid-encoded, as has been shown for the *iaaM* gen in most Psn and only a few Psv strains (Caponero et al. 1995; Zhao et al. 2005; Pérez-Martínez et al. 2008). However, while the size of the *iaaM*-encoding plasmids in Psn and Psv is highly variable among strains (65 kb to 100 kb), all Psm strains contain a native plasmid of approximately 50 kb encoding the *iaaM* gene (Figure S1). This high conservation of the plasmids, together with the monophyletic origin of the Psm genetic lineage, its close association with some Psn strains (Figure 2), and the fact that dipladenia and oleander are the only *P. savastanoi* hosts of the *Apocynaceae* family (Caballo-Ponce et al. 2017a), reinforces the hypothesis of a recent emergence of Psm strains from a Psn population (Eltlbany et al. 2012).

Psm strains are also highly homogeneous in their ability to assimilate substrates, but distinct from strains of the other four pathovars (Figure 3, Table S2). In particular, Psm strains were unable to oxidize 13 substrates assimilated by all other *P. savastanoi* strains, suggesting the loss of a large number of metabolic activities during pathovar differentiation. These differences are evident in a dendrogram from hierarchical cluster analysis of metabolic profiles, where Psm strains are clearly separated from the other pathovars and in sharp contrast with the close phylogenetic relationship between Psn and Psm strains (Figure 2, Figure S2). The discrepancy between nutritional profiles and phylogenetic relationship has also been observed with other Psv strains (Ramos et al. 2012), other *P. syringae* pathovars and nonpathogenic pseudomonads (Mithani et al. 2011; Rico and Preston, 2008), and is likely a result of host specialization. In this sense, Oksinska et al. (2011) established a link between the ability of *Pseudomonas reactans* to transform two of the substrates not oxidized by Psm strains, (*N*-acetyl-D-glucosamine and D-threalose), among other compounds, and its efficiency to colonize wheat seedlings. In addition, *thuA* and *thuB* mutants of *Sinorhizobium meliloti*, affected in trehalose catabolism, were reported to be

554 more competitive than the wild-type strain to invade alfalfa roots and form
555 nitrogen-fixing nodules (Jensen et al. 2005). Therefore, the exclusive and
556 homogeneous metabolic profile of Psm strains suggest evolutive adaptation to
557 their plant host and, together with phylogenetic analyses and plasmid-based
558 molecular methods, facilitates the unequivocal identification of *P. savastanoi*
559 strains belonging to this pathovar.

560 Our results confirm the differential host range previously reported for Psv, Psn,
561 Psf and Psr strains (Moreno-Pérez et al. 2020). They also reveal a well-defined
562 and distinctive host range for the five Psm strains, which caused disease in olive,
563 ash and dipladenia but not in oleander (Figure 4, Table 2). Psm and Psn showed
564 similar host ranges, with two of the three Psn strains examined inducing knot-like
565 overgrowths in dipladenia stems (Figure 4). However, the lack of pathogenicity of
566 Psm in the oleander cultivar we used and its natural association with dipladenia
567 are defining phenotypes separating this pathovar from Psn. Additionally,
568 pathovars Psv, Psn and Psm all induced symptoms in olive and ash. Although
569 remarkable, it is not surprising that closely related pathovars share common
570 hosts, at least in inoculations under controlled conditions. For instance, *P.*
571 *savastanoi* pv*. glycinea* R4 was isolated from a diseased soybean (*Glycine max*),
572 its natural host. However, this bacterium is also pathogenic to bean (*Phaseolus*
573 *vulgaris*) and mung bean (*Vigna radiata*), which are typical hosts of the closely
574 related pathovar *P. savastanoi* pv. *phaseolicola* (Baltrus et al. 2012). In fact,
575 overlapping host ranges appear to be a common trend in the *P. syringae* complex
576 (Morris et al. 2019). Despite this, bacteria display an ecological host range that
577 has traditionally justified their pathovar classification. In this sense, disease
578 outbreaks of MaLSS all over the world have always been associated to typical,
579 clonal Psm strains and not to bacteria from any other *P. savastanoi* pathovar.
580 This could be explained by different factors, including the dissemination of a
581 particular clone with propagative plant material or the likely requirement of various
582 genetic determinants besides T3SS that would ultimately ensure successful plant

infection, such as those involved in metabolism or competitive abilities. Our results, thus, support the notion that the novel pathovar Psm originates from an ancestral Psn lineage that lost the ability to infect oleander and specialized in infecting dipladenia plants in field conditions, causing the emergent MaLSS disease worldwide.

Here we demonstrated that Psm Ph3 caused systemic infections in dipladenia. The migration of *P. savastanoi* along the host plant has already been reported for Psv and Psn strains (Wilson 1935; Wilson and Magie 1964; Penyalver et al. 2006), taking place through xylem vessels by Psv (Maldonado-González et al. 2013; Marchi et al. 2009; Rodriguez-Moreno et al. 2009) and using the laticifers and the xylem by Psn (Wilson and Magie 1964). Since dipladenia and oleander belong to the same plant family, Psn and Psm might use a common mechanism(s) for their dissemination through the plant. When occurring, systemic infection of dipladenia causes complete wilting, a phenomenon not reported before in naturally infected plants. Nevertheless, the potential occurrence of systemic infections in the field is critically relevant for nurseries and should be taken into account during the implementation of their disease management programs.

Comparison of the Ph3 genome with those of the four sequenced Psn strains yielded 43 Ph3 singleton genes (identity <90%), 30 of which are likely plasmid-encoded (Table 3). These results suggest that Ph3 might contain a plasmid not present in any of the Psn strains examined, perhaps involved in the virulence and/or the host range of the strain. According to this, in addition to 10 hypothetical proteins, three transcriptional regulators and a gene coding for a murein-degrading enzyme were found among these singleton genes. The relevance of transcription factors in the regulation of virulence in *P. syringae* has been recently highlighted by the identification of the binding motifs of 100 transcription factors in the *P. savastanoi* pv. *phaseolicola* 1448A genome, 25 of which were demonstrated to be virulence-associated master regulators (Fan et al. 2020). On

612 the other hand, degradation and modification of peptidoglycan by murein-
613 degrading enzymes has been correlated with subversion of host immunity in
614 Gram-negative bacterial pathogens (Juan et al. 2018). Nevertheless,
615 identification of these Ph3 singleton genes in the genome of other Psm strains
616 isolated in different locations would shed light on their role as host range
617 determinants.

618 It is well known that the T3E repertoire is highly variable across strains of the
619 *P. syringae* complex (Baltrus et al. 2011; Dillon et al. 2019) and is crucial for the
620 establishment of compatible and incompatible interactions with plant hosts
621 (Jones and Dangl 2006). Although the T3E repertoires of Psn and Psm strains
622 are highly similar, several T3E sequences show truncations specifically encoded
623 by either Ph3 (HopAS1) or both Ph3 and all Psn strains (HopAO2, AvrPto1). In
624 fact, hierarchical clustering of the strains based on their T3E content revealed
625 these allelic variants to be crucial and sufficient in separating Psm Ph3 from all
626 other Psn strains (Figure 7). Nevertheless, other more subtle allelic differences
627 not considered in this study could also be relevant for the host range of Psm
628 strains. On the other hand, the inability of Psm strains to elicit an HR in *N.*
629 *tabacum* leaves might be due either to the absence of effector(s) recognized by
630 the plant immune system or to codification of specific T3E(s) suppressing
631 effector-triggered immunity in *N. tabacum*. Thus, it could be possible that the T3E
632 variants identified in Psm Ph3 are the result of the adaptation of this pathogen to
633 dipladenia to avoid recognition by the plant immune system. In this sense, the
634 observed truncations of AvrPto1 and HopAS1 in Psm Ph3 might have been
635 selected for pathogenicity in dipladenia and, at the same time, are responsible
636 for the inability of the strain to elicit an HR in tobacco leaves. In fact, AvrPto1 from
637 *P. syringae* pv. *tomato* is differentially recognized by tomato and tobacco plants,
638 as point mutations in the C-terminal region of this protein abolish the avirulence
639 in tobacco but not in tomato (Shan et al. 2000). Furthermore, while HopAS1 is
640 broadly present in *P. syringae* strains and contributes to virulence in tomato,

strains pathogenic in *Arabidopsis* carry truncated HopAS1 variants (Sohn et al. 2012). In *P. savastanoi*, T3E truncations exclusively encoded by several pathovars have been recently identified and their role in host range has been proposed (Moreno-Pérez et al. 2020).

Description of *P. savastanoi* pv. *mandevillae* pv. nov.

On LB plates, the bacterium forms circular, smooth, flat, cream-colored colonies that are resistant to 20 µg/ml nitrofurantoin. On KB plates, colonies are weakly fluorescent under UV light. Unlike most *P. savastanoi*, strains were negative for all LOPAT tests (levan production, oxidase, arginine dihydrolase, pectinolytic activity, and tobacco hypersensitivity). However, MLSA of concatenated partial sequences of *gyrB*, *rpoD*, *gapA*, *rpoA* and *recA* genes place the strains in phylogroup 3 (genomospecies 2) of the *P. syringae* complex clustering in a monophyletic lineage and, together with Psn strains, in a distinct clade that is well-separated from strains of the remaining *P. savastanoi* pathovars. Strains yield an amplicon of approximately 1.1 kb in PCR tests targeting the 3' end of gene *repA* and the 5' end of gene *rulA*, whereas other *P. savastanoi* strains produce smaller bands or no specific amplicons (Eltlbany et al. 2012). In Biolog GN2 plates, the strains are impaired in the transformation of 13 compounds that are partially or completely oxidized by strains of the other four *P. savastanoi* pathovars, *i.e.* N-acetyl-D-glucosamine, L-fucose, maltose, D-melibiose, L-rhamnose, D-trehalose, D,L-lactic acid, D-serine, uridine, thymidine, 2-Aminoethanol, α-D-glucose-1-phosphate, D-glucose-6-phosphate. Strains of Psm are differentiated from the other four *P. savastanoi* pathovars of woody hosts by knot formation on dipladenia (*Mandevilla* spp., natural host), olive (*Olea europaea*) and ash (*Fraxinus excelsior*), and because they are not pathogenic in broom (*Retama sphaerocarpa*) and oleander (*Nerium oleander*) accession "white". The pathotype strain of pathovar mandevillae is Ph3 (syn. CFBP8832^{PT}).

669 ## ACKNOWLEDGMENTS

670 We thank T. Dreo (National Institute of Biology, Slovenia), M.L. Putnam
671 (Oregon State University) and A. Oder for the supply of Psm NIB Z 1413, Psm
672 1397 and dipladenia plants, respectively, P. Rodríguez-Palenzuela, L. Díaz and
673 J. Sánchez-Colmenero for help with bioinformatics pipelines, P. García-Vallejo,
674 for technical assistance, A. Macho and C. Beuzón for providing plasmid pAME8
675 and T.H. Osinga for advice on English usage. We are indebted to J.A. Torés for
676 his invaluable help with Latin in naming the new pathovar.

677

LITERATURE CITED

Alvarez, F., García de los Ríos, J. E., Jimenez, P., Rojas, A., Reche, P., and Troya, M. T. 1998. Phenotypic variability in different strains of *Pseudomonas syringae* subsp. savastanoi isolated from different hosts. Eur. J. Plant Pathol. 104:603-609.

Añorga, M., Pintado, A., Ramos, C., De Diego, N., Ugena, L., Novák, O., and Murillo, J. 2020. Genes *ptz* and *idi*, coding for cytokinin biosynthesis enzymes, are essential for tumorigenesis and *in planta* growth by *P. syringae* pv. savastanoi NCPPB 3335. Front. Plant Sci. 11:1294.

Aragón, I. M., Pérez-Martínez, I., Moreno-Pérez, A., Cerezo, M., and Ramos, C. 2014. New insights into the role of indole-3-acetic acid in the virulence of *Pseudomonas savastanoi* pv. savastanoi. FEMS Microbiol. Lett. 356:184-192.

Balestra, G. M., Lamichhane, J. R., Kshetri, M. B., Mazzaglia, A., and Varvaro, L. 2009. First report of olive knot caused by *Pseudomonas savastanoi* pv. savastanoi in Nepal. Plant Pathol. 58:393.

Baltrus, D. A., Nishimura, M. T., Romanchuk, A., Chang, J. H., Mukhtar, M. S., Cherkis, K., Roach, J., Grant, S. R., Jones, C. D., and Dangl, J. L. 2011. Dynamic evolution of pathogenicity revealed by sequencing and comparative genomics of 19 *Pseudomonas syringae* isolates. PLoS Pathog. 7:e1002132.

Baltrus, D. A., Nishimura, M. T., Dougherty, K. M., Biswas, S., Mukhtar, M. S., Vicente, J., Holub, E. B., and Dangl, J. L. 2012. The molecular basis of host specialization in bean pathovars of *Pseudomonas syringae*. Mol. Plant-Microbe Interact. 25:877-888.

Berge, O., Monteil, C. L., Bartoli, C., Chandeysson, C., Guilbaud, C., and Sands, D. C. 2014. A user's guide to a data base of the diversity of *Pseudomonas syringae* and its application to classifying strains in this phylogenetic complex. PLoS ONE 9:e105547.

Bertani, G. 1951. STUDIES ON LYSOGENESIS I. The mode of phage liberation by lysogenic *Escherichia coli*. J. Bacteriol. 62:293-300.

Bull, C. T., De Boer, S. H., Denny, T. P., Firrao, G., Fischer-Le Saux, M., Saddler, G. S., Scortichini, M., Stead, D. E., and Takikawa, Y. 2010. Comprehensive list of names of plant pathogenic bacteria, 1980–2007. J. Plant Pathol. 92:551-592.

Caballo-Ponce, E., and Ramos, C. 2016. First Report of Dipladenia (*Mandevilla* spp.) Leaf and Stem Spot Caused by *Pseudomonas savastanoi* in Spain. Plant Dis. 100:2319.

Caballo-Ponce, E., Murillo, J., Martínez-Gil, M., Moreno-Pérez, A., Pintado, A., and Ramos, C. 2017a. Knots untie: molecular determinants involved in knot formation induced by *Pseudomonas savastanoi* in woody hosts. Front. Plant Sci. 8:1089.

Caballo-Ponce, E., van Dillewijn, P., Wittich, R.M., and Ramos, C. 2017b. WHOP, a genomic region associated with woody hosts in the *Pseudomonas syringae* complex contributes to the virulence and fitness of *Pseudomonas savastanoi* pv. savastanoi in olive plants. Mol. Plant-Microbe Interact. 30: 113-126.

Caponero, A., Contesini, A. M., and Iacobellis, N. S. 1995. Population diversity of Pseudomonas syringae subsp. savastanoi on olive and oleander. Plant Pathol. 44:848-855.

Carver, T., Harris, S. R., Berriman, M., Parkhill, J., and McQuillan, J. A. 2012. Artemis: an integrated platform for visualization and analysis of high-throughput sequence-based experimental data. Bioinformatics 28:464-469.

Casimiro-Soriguer, C. S., Muñoz-Mérida, A., and Pérez-Pulido, A. J. 2017. Sma3s: A universal tool for easy functional annotation of proteomes and transcriptomes. Proteomics 17:1700071.

735 Chaudhari, N., Gupta, V., and Dutta, C. 2016. BPGA- an ultra-fast pan-genome
736 analysis pipeline. Sci. Rep. 6:24373.
737 Dillon, M. M., Thakur, S., Almeida, R. N. D., Wang, P. W., Weir, B. S., and
738 Guttman, D. S. 2019. Recombination of ecologically and evolutionarily
739 significant loci maintains genetic cohesion in the *Pseudomonas syringae*
740 species complex. Genome Biol. 20:3.
741 Dye, D. W., Bradbury, J. F., Goto, M., Hayward, A. C., Lelliott, R. A., and Schroth,
742 M. N. 1980. International standards for naming pathovars of
743 phytopathogenic bacteria and a list of pathovar names and pathotype
744 strains. Rev. Plant Pathol. 59:153-168.
745 Edgar, R. C. 2010. Search and clustering orders of magnitude faster than BLAST.
746 Bioinformatics 26:2460-2461.
747 Eltlbany, N., Prokscha, Z. Z., Castaneda-Ojeda, M. P., Krogerrecklenfort, E.,
748 Heuer, H., Wohanka, W., Ramos, C., and Smalla, K. 2012. A new bacterial
749 disease on *Mandevilla sanderi*, caused by *Pseudomonas savastanoi*:
750 lessons learned for bacterial diversity studies. Appl. Environ. Microbiol.
751 78:8492-8497.
752 Fan, L., Wang, T., Hua, C., Sun, W., Li, X., Grunwald, L., Liu, J., Wu, N., Shao,
753 X., Yin, Y., Yan, J., and Deng, X. 2020. A compendium of DNA-binding
754 specificities of transcription factors in *Pseudomonas syringae*. Nature
755 Communications 11:4947.
756 Gardan, L., Bollet, C., Abu Ghorrah, M., Grimont, F., and Grimont, P. A. D. 1992.
757 DNA relatedness among the pathovar strains of *Pseudomonas syringae*
758 subsp. savastanoi Janse (1982) and proposal of *Pseudomonas*
759 *savastanoi* sp. nov. Int. J. Syst. Bacteriol. 42:606-612.
760 Gomila, M., Busquets, A., Mulet, M., García-Valdés, E., and Lalucat, J. 2017.
761 Clarification of taxonomic status within the *Pseudomonas syringae*
762 species group based on a phylogenomic analysis. Front. Microbiol.
763 8:2422.

764 Gordon, S. A., and Weber, R. P. 1951. Colorimetric estimation of indoleacetic
765 acid. Plant Physiol. 26:192-195.
766 Gori, A., Cerboneschi, M., and Tegli, S. 2012. High-resolution melting analysis as
767 a powerful tool to discriminate and genotype *Pseudomonas savastanoi*
768 pathovars and strains. PLoS ONE 7:e30199.
769 Gutiérrez-Barranquero, J. A., Carrión, V. J., Murillo, J., Arrebola, E., Arnold, D.
770 L., Cazorla, F. M., and de Vicente, A. 2013. A *Pseudomonas syringae*
771 diversity survey reveals a differentiated phylotype of the pathovar *syringae*
772 associated with the mango host and mangotoxin production. 103:1115-
773 1129.
774 Hanahan, D. 1983. Studies on transformation of *Escherichia coli* with plasmids.
775 J. Mol. Biol. 166:557-580.
776 Hosni, T., Moretti, C., Devescovi, G., Suarez-Moreno, Z. R., Fatmi, M. B.,
777 Guarnaccia, C., Pongor, S., Onofri, A., Buonaurio, R., and Venturi, V.
778 2011. Sharing of quorum-sensing signals and role of interspecies
779 communities in a bacterial plant disease. ISME J. 5:1857-1870.
780 Hueck, C. J. 1998. Type III protein secretion systems in bacterial pathogens of
781 animals and plants. Microbiol. Mol. Biol. Rev. 62:379-433.
782 Iacobellis, N. S., Caponero, A., and Evidente, A. 1998. Characterization of
783 *Pseudomonas syringae* ssp. *savastanoi* strains isolated from ash. Plant
784 Pathol. 47:73-83.
785 Janse, J. D. 1981. The bacterial disease of ash (*Fraxinus excelsior*), caused by
786 *Pseudomonas syringae* subsp. *savastanoi* pv. fraxini. II. Etiology and
787 taxonomic considerations. Eur. J. Forest Pathol. 11:425-438.
788 Janse, J. D. 1982. *Pseudomonas syringae* subsp. *savastanoi* (ex Smith) subsp.
789 nov., nom. rev., the bacterium causing excrescences on *Oleaceae* and
790 *Neriurn oleander* L. Int. J. Syst. Evol. Microbiol. 32:166-169.

Janse, J. D. 1991. Pathovar discrimination within *Pseudomonas syringae* subsp. *savastanoi* using whole cell fatty acids and pathogenicity as criteria. Syst. Appl. Microbiol. 14:79-84.

Jensen, J. B., Ampomah, O. Y., Darrah, R., Peters, N. K., and Bhuvaneswari, T. V. 2005. Role of trehalose transport and utilization in *Sinorhizobium meliloti*-Alfalfa interactions. Mol. Plant-Microbe Interact. 18:694-702.

Jones, J. D., and Dangl, J. L. 2006. The plant immune system. Nature 444:323-329.

Juan, C., Torrens, G., Barceló, I.M. and Oliver, A. 2018. Interplay between peptidoglycan biology and virulence in gram-negative pathogens. Microbiol. Mol. Biol. Rev. 82: e00033-18.

Kearse, M., Moir, R., Wilson, A., Stones-Havas, S., Cheung, M., Sturrock, S., Buxton, S., Cooper, A., Markowitz, S., Duran, C., Thierer, T., Ashton, B., Meintjes, P., and Drummond, A. 2012. Geneious Basic: an integrated and extendable desktop software platform for the organization and analysis of sequence data. Bioinformatics 28:1647-1649.

King, E. O., Ward, M. K., and Raney, D. E. 1954. Two simple media for the demonstration of pyocyanin and fluorescin. J. Lab. Clin. Med. 44:301-307.

Kumar, S., Stecher, G., and Tamura, K. 2016. MEGA7: molecular evolutionary genetics analysis version 7.0 for bigger datasets. Mol. Biol. Evol. 33:1870-1874.

Lamichhane, J. R., Varvaro, L., Parisi, L., Audergon, J.-M., and Morris, C. E. 2014. Disease and frost damage of woody plants caused by *Pseudomonas syringae*: seeing the forest for the trees. Pages 235-295 in: Advances in Agronomy, vol. 126. D. L. Sparks, ed. Academic Press, San Diego, CA.

Lee, I., Ouk Kim, Y., Park, S.-C., and Chun, J. 2016. OrthoANI: An improved algorithm and software for calculating average nucleotide identity. Int. J. Syst. Evol. Microbiol. 66:1100-1103.

820 Lelliott, R. A., Billing, E., and Hayward, A. C. 1966. A determinative scheme for
821 the fluorescent plant pathogenic pseudomonads. J. Appl. Bacteriol.
822 29:470-489.
823 Macho, A. P., Ruiz-Albert, J., Tornero, P., and Beuzón, C. R. 2009. Identification
824 of new type III effectors and analysis of the plant response by competitive
825 index. Mol. Plant Pathol. 10:69-80.
826 Maldonado-González, M. M., Prieto, P., Ramos, C., and Mercado-Blanco, J.
827 2013. From the root to the stem: interaction between the biocontrol root
828 endophyte *Pseudomonas fluorescens* PICF7 and the pathogen
829 *Pseudomonas savastanoi* NCPPB 3335 in olive knots. Microb. Biotechnol.
830 6:275-287.
831 Marchi, G., Mori, B., Pollacci, P., Mencuccini, M., and Surico, G. 2009. Systemic
832 spread of *Pseudomonas savastanoi* pv. savastanoi in olive explants. Plant
833 Pathol. 58:152-158.
834 Martínez-García, P. M., Ramos, C., and Rodríguez-Palenzuela, P. 2015.
835 T346Hunter: a novel web-based tool for the prediction of type III, type IV
836 and type VI secretion systems in bacterial genomes. PLoS ONE
837 10:e0119317.
838 Martínez-García, P. M., López-Solanilla, E., Ramos, C., and Rodríguez-
839 Palenzuela, P. 2016. Prediction of bacterial associations with plants using
840 a supervised machine-learning approach. Environ. Microbiol. 18:4847-
841 4861.
842 Mithani, A., Hein, J., and Preston, G. M. 2011. Comparative analysis of metabolic
843 networks provides insight into the evolution of plant pathogenic and
844 nonpathogenic lifestyles in *Pseudomonas*. Mol. Biol. Evol. 28:483-499.
845 Moreno-Pérez, A., Pintado, A., Murillo, J., Caballo-Ponce, E., Tegli, S., Moretti,
846 C., Rodríguez-Palenzuela, P., and Ramos, C. 2020. Host range
847 determinants of *Pseudomonas savastanoi* pathovars of woody hosts

revealed by comparative genomics and cross-pathogenicity tests. Front. Plant Sci. 11:973.

Moretti, C., Vinatzer, B. A., Onofri, A., Valentini, F., and Buonaurio, R. 2017. Genetic and phenotypic diversity of Mediterranean populations of the olive knot pathogen, *Pseudomonas savastanoi* pv. *savastanoi*. Plant Pathol. 66:595-605.

Morris, C. E., Lamichhane, J. R., Nikolić, I., Stanković, S., and Moury, B. 2019. The overlapping continuum of host range among strains in the *Pseudomonas syringae* complex. Phytopathol. Res. 1:4.

Mudgett, M. B., and Staskawicz, B. J. 1999. Characterization of the *Pseudomonas syringae* pv. tomato AvrRpt2 protein: demonstration of secretion and processing during bacterial pathogenesis. Mol. Microbiol. 32:927-941.

Murillo, J., and Keen, N. T. 1994. Two native plasmids of *Pseudomonas syringae* pathovar tomato strain PT23 share a large amount of repeated DNA, including replication sequences. Mol. Microbiol. 12:941-950.

Nowell, R. W., Laue, B. E., Sharp, P. M., and Green, S. 2016. Comparative genomics reveals genes significantly associated with woody hosts in the plant pathogen *Pseudomonas syringae*. Mol. Plant Pathol. 17:1409-1424.

Oder, A., Lannes, R., and Viruel, M. A. 2016. A set of 20 new SSR markers developed and evaluated in *Mandevilla* Lindl. Molecules 21:1316.

Oksinska, M. P., Wright, S. A. I., and Pietr, S. J. 2011. Colonization of wheat seedlings (*Triticum aestivum* L.) by strains of *Pseudomonas* spp. with respect to their nutrient utilization profiles. Eur. J. Soil Biol. 47:364-373.

Peeters, N., Carrère, S., Anisimova, M., Plener, L., Cazalé, A.-C., and Genin, S. 2013. Repertoire, unified nomenclature and evolution of the type III effector gene set in the *Ralstonia solanacearum* species complex. BMC Genomics 14:859.

876 Penyalver, R., Garcia, A., Ferrer, A., Bertolini, E., Quesada, J. M., Salcedo, C. I.,
877 Piquer, J., Perez-Panades, J., Carbonell, E. A., Del Rio, C., Caballero, J.
878 M., and Lopez, M. M. 2006. Factors affecting *Pseudomonas savastanoi*
879 pv. savastanoi plant inoculations and their use for evaluation of olive
880 cultivar susceptibility. Phytopathology 96:313-319.
881 Pérez-Martínez, I., Rodríguez-Moreno, L., Matas, I. M., and Ramos, C. 2007.
882 Strain selection and improvement of gene transfer for genetic manipulation
883 of *Pseudomonas savastanoi* isolated from olive knots. Res. Microbiol.
884 158:60-69.
885 Pérez-Martínez, I., Zhao, Y., Murillo, J., Sundin, G. W., and Ramos, C. 2008.
886 Global genomic analysis of *Pseudomonas savastanoi* pv. savastanoi
887 plasmids. J. Bacteriol. 190:625-635.
888 Pirc, M., Ravnikar, M., and Dreo, T. 2015. First Report of *Pseudomonas*
889 *savastanoi* Causing Bacterial Leaf Spot of *Mandevilla sanderi* in Slovenia.
890 Plant Dis. 99:415-415.
891 Putnam, M. L., Curtis, M., Serdani, M., and Palmateer, A. J. 2010. *Pseudomonas*
892 *savastanoi* found in association with stem galls on *Mandevilla*.
893 Phytopathology 100:S104.
894 Ramos, C., Matas, I. M., Bardaji, L., Aragon, I. M., and Murillo, J. 2012.
895 *Pseudomonas savastanoi* pv. savastanoi: some like it knot. Mol. Plant
896 Pathol. 13:998-1009.
897 Rico, A., and Preston, G. M. 2008. *Pseudomonas syringae* pv. tomato DC3000
898 uses constitutive and apoplast-induced nutrient assimilation pathways to
899 catabolize nutrients that are abundant in the tomato apoplast. Mol. Plant-
900 Microbe Interact. 21:269-282.
901 Rodriguez-Moreno, L., Jimenez, A. J., and Ramos, C. 2009. Endopathogenic
902 lifestyle of *Pseudomonas savastanoi* pv. savastanoi in olive knots. Microb.
903 Biotechnol. 2:476-488.

Sato, M., Staskawicz, B. J., and Panopoulos, N. J. 1982. Indigenous plasmids of *Pseudomonas syringae* pv. *mori*, the causal agent of bacterial blight of mulberry. Jpn. J. Phytopathol. 48:27-33.

Shan, L., Thara, V. K., Martin, G. B., Zhou, J.-M., and Tang, X. 2000. The pseudomonas AvrPto protein is differentially recognized by tomato and tobacco and is localized to the plant plasma membrane. Plant Cell 12:2323-2337.

Sohn, K. H., Saucet, S. B., Clarke, C. R., Vinatzer, B. A., O'Brien, H. E., Guttman, D. S., and Jones, J. D. G. 2012. HopAS1 recognition significantly contributes to *Arabidopsis* nonhost resistance to *Pseudomonas syringae* pathogens. New Phytol. 193:58-66.

Surico, G., Iacobellis, N. S., and Sisto, A. 1985. Studies on the role of indole-3-acetic acid and cytokinins in the formation of knots on olive and oleander plants by *Pseudomonas syringae* pv. savastanoi. Physiol. Plant Pathol. 26:309-320.

Tegli, S., Cerboneschi, M., Marsili Libelli, I., and Santilli, E. 2010. Development of a versatile tool for the simultaneous differential detection of *Pseudomonas savastanoi* pathovars by End Point and Real-Time PCR. BMC Microbiol. 10:156.

Tegli, S., Gori, A., Cerboneschi, M., Cipriani, M. G., and Sisto, A. 2011. Type three secretion system in *Pseudomonas savastanoi* pathovars: does timing matter? Genes 2:957.

Tegli, S., Bini, L., Calamai, S., Cerboneschi, M., and Biancalani, C. 2020. A MATE transporter is involved in pathogenicity and IAA homeostasis in the hyperplastic plant pathogen *Pseudomonas savastanoi* pv. nerii. Microorganisms 8:156.

Treangen, T. J., Ondov, B. D., Koren, S., and Phillippy, A. M. 2014. The Harvest suite for rapid core-genome alignment and visualization of thousands of intraspecific microbial genomes. Genome Biol. 15:524.

933 Ullrich, M., Bereswill, S., Volksch, B., Fritsche, W., and Geider, K. 1993.
934 Molecular characterization of field isolates of *Pseudomonas syringae* pv.
935 *glycinea* differing in coronatine production. J. Gen. Microbiol. 139:1927-
936 1937.
937 von Bodman, S. B., and Shaw, P. D. 1987. Conservation of plasmids among
938 plant-pathogenic *Pseudomonas syringae* isolates of diverse origins.
939 Plasmid 17:240-247.
940 Wilson, E. 1935. The olive knot disease: its inception, development, and control.
941 Hilgardia 9:231-264.
942 Wilson, E., and Magie, A. 1964. Systemic invasion of the host plant by the tumor-
943 inducing bacterium, *Pseudomonas savastanoi*. Phytopathology 54:577–
944 579.
945 Zhao, Y., Ma, Z., and Sundin, G. W. 2005. Comparative genomic analysis of the
946 pPT23A plasmid family of *Pseudomonas syringae*. J. Bacteriol. 187:2113-
947 2126.
948 Zhou, C., Yang, Y., and Jong, A. Y. 1990. Mini-prep in ten minutes. Biotechniques
949 8:172-173.
950

951 **Table 1.** Wild-type *Pseudomonas savastanoi* strains used in this study

Strain (syn.)[a]	Host of isolation	Country of isolation	Year of isolation	Reference
pv. *fraxini*				
NCPPB 1464	*Fraxinus excelsior*	United Kingdom	1963	Janse (1981)
NCPPB 1006	*F. excelsior*	United Kingdom	1961	Janse (1981)
CFBP 5062	*F. excelsior*	The Netherlands	1978	Janse (1991)
pv. *mandevillae*				
Ph3 (CFBP 8832)	*Mandevilla sanderi*	France	2008	Eltlbany et al. (2012)
MSI13L (CFBP 8835)	*Mandevilla* spp.	Spain	2013	Caballo-Ponce and Ramos (2016)
Ph5 (CFBP 8833)	*M. sanderi*	Germany	2008	Eltlbany et al. (2012)
1397	*M. splendens*	United States	2010	Putnam et al. (2010)
NIB Z 1413	*M. sanderi*	Slovenia	2010	Pirc et al. (2015)
pv. *nerii*				
Psn23	*Nerium oleander*	Italy	2004	Tegli et al. (2011)
CFBP 5067	*N. oleander*	Spain	2007	Janse (1991)
ITM 519 (ICMP 13546)	*N. oleander*	Italy	Before 1985	Surico et al. (1985)
pv. *savastanoi*				
NCPPB 3335	*Olea europaea*	France	1984	Pérez-Martínez et al. (2007)/D.E. Stead
CFBP 1670	*O. europaea*	Italy	Before 1959	D. Sutic
PseNe107	*O. europaea*	Nepal	2007	Balestra et al. (2009)
DAPP-PG722	*O. europaea*	Italy	2007	Hosni et al. (2011)
pv. *retacarpa*				
CECT 4861	*Retama sphaerocarpa*	Spain	1996	Alvarez et al. (1998)

952 [a]pv, pathovar; syn., synonymous name in other bacterial collections; NCPPB,
953 National Collection of Plant Pathogenic Bacteria (United Kingdom); CFBP,
954 French Collection of Plant-associated Bacteria.
955

956 **Table 2.** Cross-pathogenicity tests of *P. savastanoi* strains isolated from

957 dipladenia or diverse woody hosts.

Host of isolation/Strain[a]	Dipladenia[b]	Olive[b]	Oleander[b]	Ash[b]	Broom[b]
Dipladenia					
Psm Ph3	10K	10K	-	10S	-
Psm MSI13L	10K	10K	-	5S 5K	-
Psm Ph5	10K	10K	-	1S 9K	-
Psm 1397	10K	10K	-	9S 1K	-
Psm NIB Z 1413	10K	10K	-	8S 2K	-
Olive					
Psv NCPPB 3335	-	10K	-	10S	-
Oleander					
Psn *Psn23*	-	1S 9K	8K 2E	10S	-
Ash					
Psf NCPPB 1006	-	-	-	10E	-
Broom					
Psr CECT 4861	-	-	-	10S	10K

958 [a]Dipladenia, *Mandevilla* spp.; olive, *Olea europaea*; oleander, *Nerium oleander*;
959 ash, *Fraxinus excelsior*; broom, *Retama sphaerocarpa*; Psm, Psv, Psn, Psf, and
960 Psr, *P. savastanoi* pathovars *mandevillae*, *savastanoi*, *nerii*, *fraxini*, and
961 *retacarpa*, respectively.

962 [b]K, Knot; S, swelling; E, excrescence; -, similar to the negative control (plants
963 inoculated with 10 mM $MgCl_2$). For each host and strain, numbers indicate the
964 amount of a particular symptom generated out of 10 inoculation points.

965

966 **Table 3.** Strain-specific proteins identified in *P. savastanoi* pv. *mandevillae* Ph3

967 classified into functional categories.

Protein ID[a]	Description
DNA replication, recombination, mutation and repair	
WP_058886974	Prophage PssSM-03, GDSL-like lipase/acylhydrolase family protein
WP_080719059	Putative ATP-dependent helicase
WP_095178651	Transposase IS*Psy4*
WP_095178747	MobC
WP_095178748	Nickase
WP_095178772	Putative Rep protein
WP_095178774	ParA-like partition protein
WP_095178775	ParB-like partition protein
WP_095178777	Resolvase
WP_095178897	Tyrosine recombinase XerC
Metabolism	
WP_095178718	ATP phosphoribosyltransferase
WP_095178778	Membrane-bound lytic murein transglycosylase C
Toxins, antitoxins	
WP_095178754	Type II toxin-antitoxin system RelE/ParE family toxin
WP_095178755	Putative addiction module antidote protein
Secretion System	
WP_095178757	Type IV secretion system protein (VirD4)
WP_095178758	Type IV secretion system protein (VirB11)
WP_095178760	Type IV secretion system protein (VirB9)
WP_095178761	Type IV secretion system protein (VirB8)
WP_095178762	Type IV secretion system protein (VirB6)
WP_095178765	Type IV secretion system protein (VirB4)
WP_095178767	Type IV secretion system protein (VirB2)
WP_176467475	Type IV secretion system protein (VirB5)
Transcriptional regulator	
WP_095178756	Putative transcriptional regulator
WP_095178773	TrfB protein

WP_095178779	Transcription elongation protein (SprT domain)
Hypothetical Protein	
WP_005754776, **WP_095178749**, **WP_095178750**, **WP_095178751**, **WP_095178752**, **WP_095178753**, **WP_095178768**, **WP_095178769**, **WP_095178770**, **WP_095178771**, **WP_095178776**, WP_095178834, WP_095178863, WP_095178905, WP_095178907, WP_095178908, WP_095178957, WP_095179008	

968 [a]Bolded protein numbers indicate products from genes encoded in contig

969 NZ_NIAX01000040 (27720 nt).

970

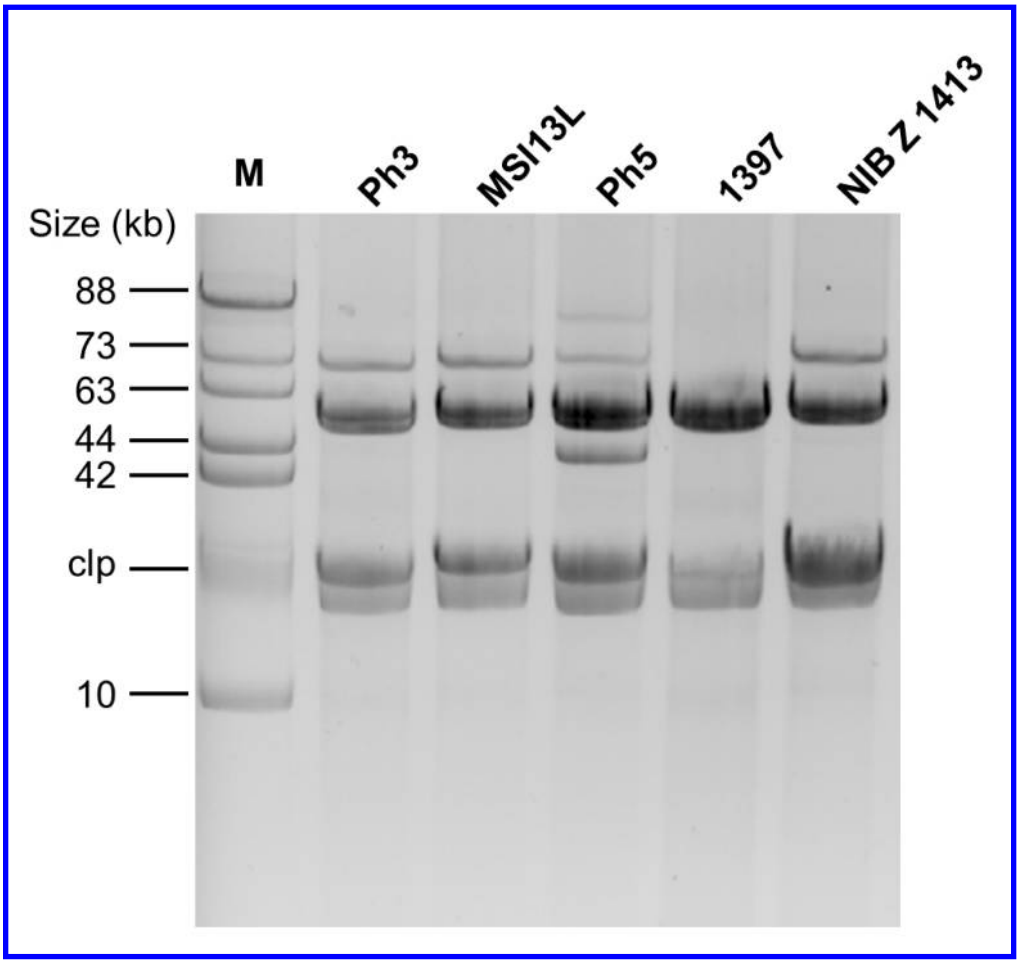

Figure 1. Plasmid profile of *P. savastanoi* pv. *mandevillae* strains isolated in different countries. Native plasmids of *P. savastanoi* pv. *savastanoi* ITM 317 (M) were used as DNA molecular size marker. clp, chromosome and linearized plasmids. Strains are described in Table 1.

85x80mm (300 x 300 DPI)

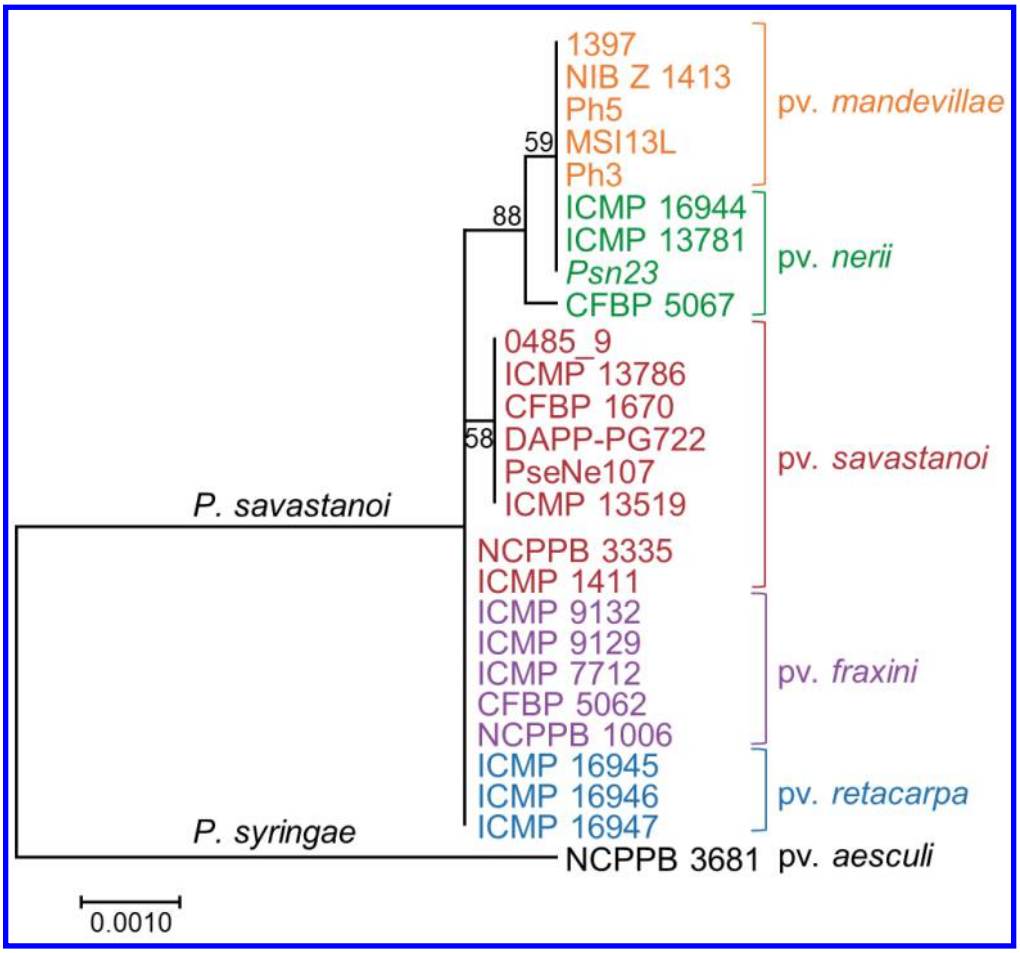

Figure 2. Phylogenetic analysis of *P. savastanoi* strains isolated from diverse woody hosts. The tree was constructed using MEGA7 (Kumar et al. 2016) with the maximum-likelihood method and concatenated partial sequences of *gyrB*, *rpoD*, *gapA*, *rpoA* and *recA* genes (total length 3219 nt). The tree was rooted with *P. syringae* pv. *aesculi* NCPPB 3681.

85x78mm (300 x 300 DPI)

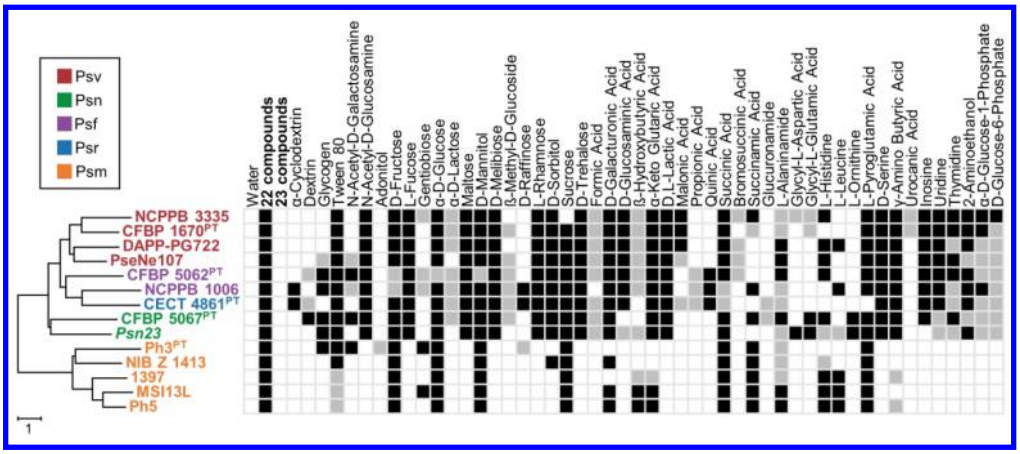

Figure 3. Hierarchical clustering of *P. savastanoi* strains based on their metabolic profiles. The similarity matrix was constructed using Euclidean distance with Morpheus software; cluster analysis was performed with the neighbor-joining method using MEGA7 (Kumar et al. 2016). The scale represents the linkage distance. Black, gray, and white boxes indicate complete, partial, and negative oxidation of the substrate, respectively. The 22 and 23 substrates showing for all the strains tested complete and negative oxidation, respectively, are indicated in Table S2.

178x76mm (300 x 300 DPI)

Figure 4. Cross pathogenicity tests of *P. savastanoi* strains. (A) Symptoms most frequently generated by *P. savastanoi* strains at 90 days post-inoculation (dpi) in olive, oleander, ash, broom and dipladenia (see Table 2 for details). 5 Psm strains: *P. savastanoi* pv. *mandevillae* (Psm) Ph3, MSI13L, Ph5, 1397 and NIBZ1413. (B) Symptoms induced in dipladenia stems by the indicated *P. savastanoi* strains at 90 dpi. Psn, Psv, Psf and Psr, *P. savastanoi* pathovars *nerii*, *savastanoi, fraxini*, and *retacarpa*, respectively. $MgCl_2$, negative control plants inoculated with 10 mM $MgCl_2$; +, virulent strain in the corresponding host; -, strain inducing no symptoms (similar to the negative control plants).

178x181mm (300 x 300 DPI)

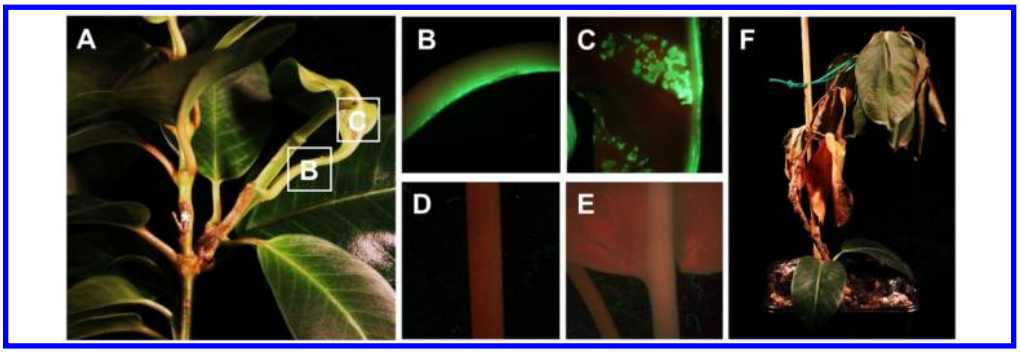

Figure 5. Systemic infection caused by *P. savastanoi* pv. *mandevillae* (Psm) Ph3 on dipladenia plants. (A) Development of secondary symptoms induced at 23 days post-inoculation by the GFP-tagged derivative of Ph3-GFP. The asterisk indicate the inoculation point. White boxes correspond to the petiole and leaf areas whose epifluorescence images are shown in (B) and (C), respectively. (D) and (E), epifluorescence images of a petiole and leaf from a non-infected dipladenia plant (negative control). The red background in these images is due to chlorophyll fluorescence. (F) Bacterial wilt of dipladenia plants infected with Psm Ph3 at 90 days post-inoculation.

178x59mm (300 x 300 DPI)

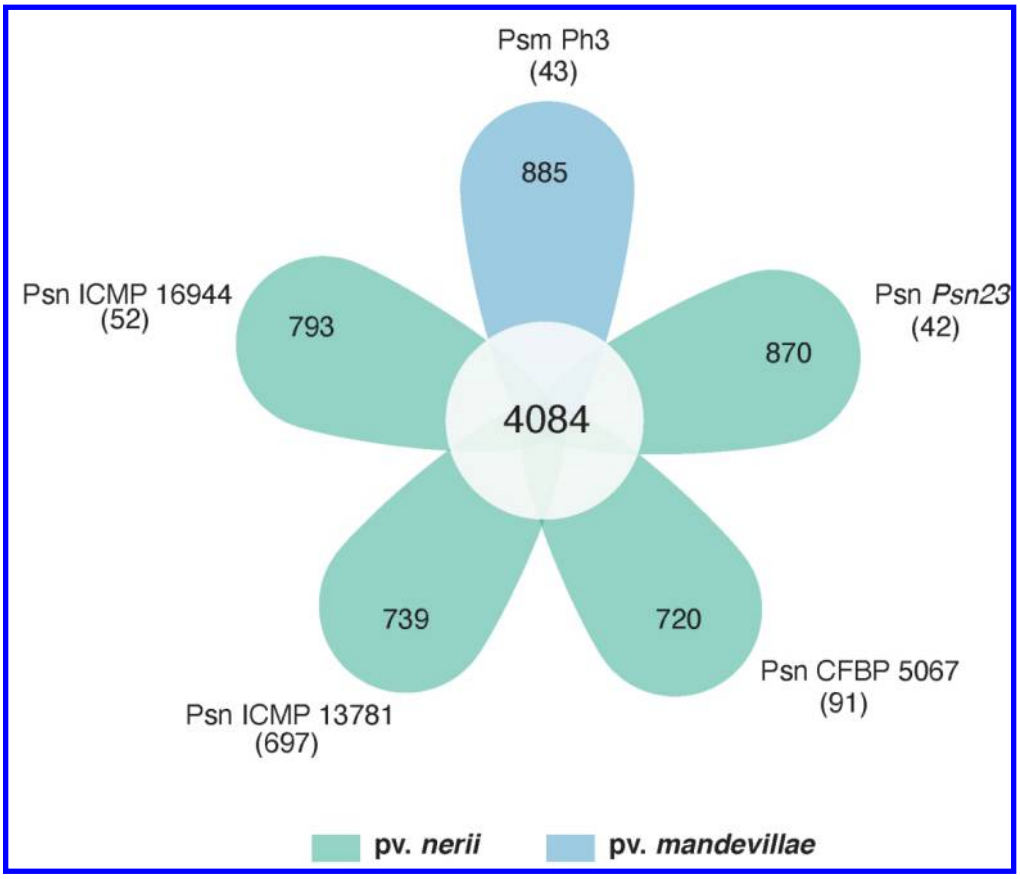

Figure 6. Comparative genomic analysis of *P. savastanoi* pv. *nerii* (Psn) and *P. savastanoi* pv. *mandevillae* (Psm) strains. The flower plot diagram represents the number of genes in the core-genome (center), the accessory genes (petals) and the strain-specific genes (in brackets). Numbers were calculated using the pan-genome analysis tool BPGA (Chaudhari et al. 2016).

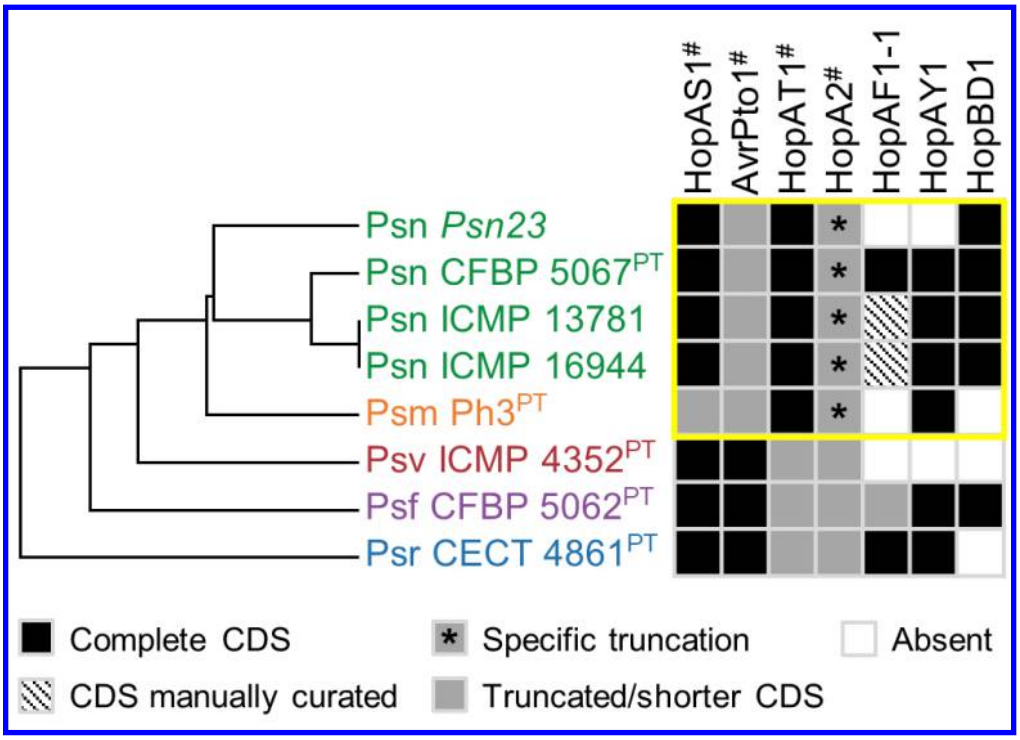

Figure 7. Distribution of T3SS effectors differentially encoded by *P. savastanoi* pv. *mandevillae* (Psm) and *P. savastanoi* pv. *nerii* (Psn). The yellow square frames T3SS effectors (T3Es) differentially encoded between Psm Ph3 and Psn strains (HopaAS1, HopAF1-1, HopAY1 and HopBD1) and T3Es that Psm Ph3 and Psn strains encode differently than the other three *P. savastanoi* pathovars of woody hosts (AvrPto1, HopAT1 and HopA2). The hierarchical clustering tree of *P. savastanoi* strains based on their T3E repertories (left) was generated using Morpheus. All sequenced strains of Psm and Psn, as well as a representative strain of P. savastanoi pathovars *savastanoi* (Psv), *fraxini* (Psf) and *retacarpa* (Psr) were included in this analysis. The asterisks indicate a specific truncation of HopA2 only found in Psm Ph3 and Psn strains, different from that encoded by all other sequenced *P. savastanoi* strains. PT, pathotype strain; #, T3SS effectors included in the core genome of Psm Ph3 and Psn strains.

85x60mm (300 x 300 DPI)

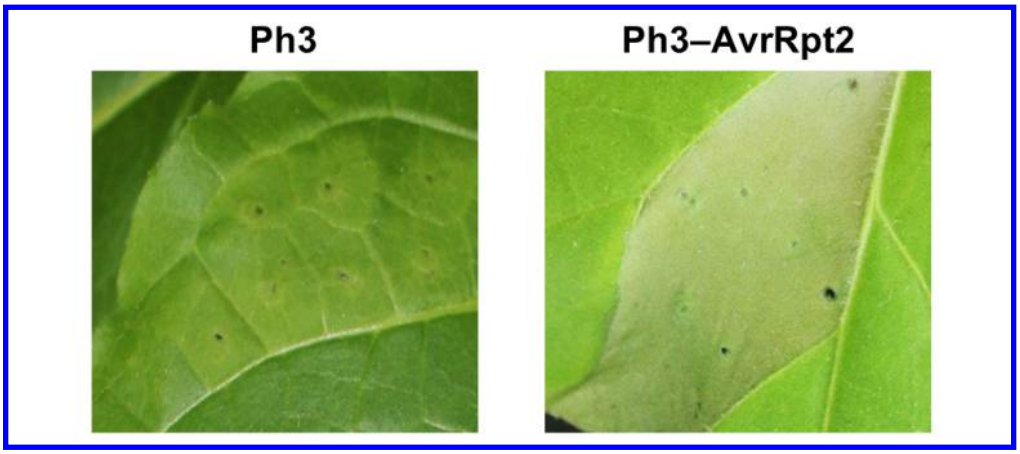

Figure 8. Restoration of HR elicitation to *P. savastanoi* pv. *mandevillae* Ph3 in tobacco leaves by heterologous expression of the T3SS effector AvrRpt2. Hypersensitive response (HR) of *Nicotiana tabacum* cv. Xanthi leaves 48h after infection with wild-type Ph3 or Ph3 expressing the T3SS effector AvrRpt2 from *P. syringae* pv. *tomato* 1065 (Ph3-AvrRpt2).

85x36mm (300 x 300 DPI)

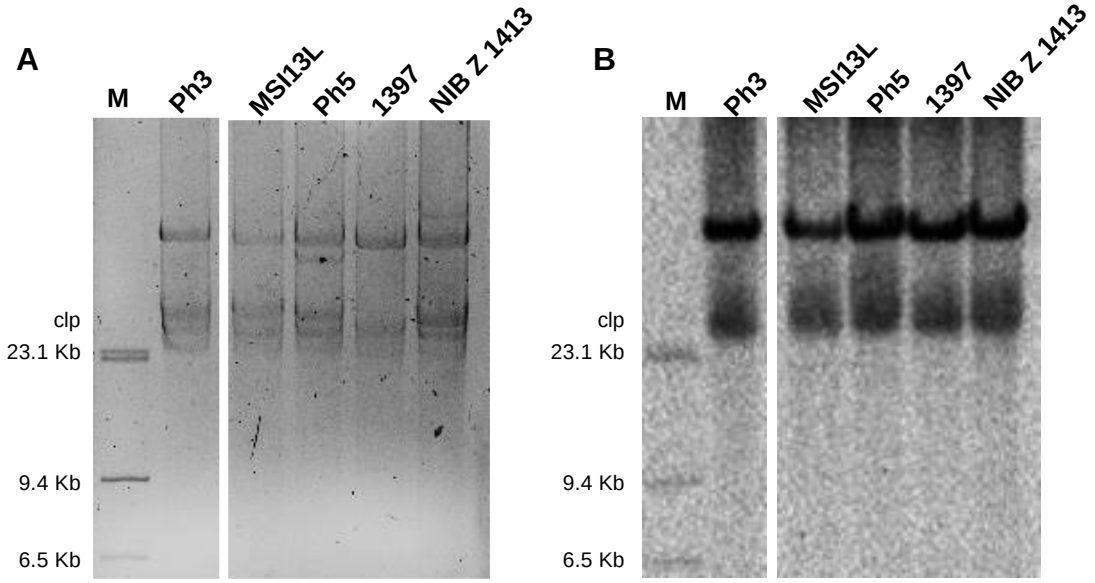

Figure S1. Localization of the *iaaM* gene in a native plasmid of *P. savastano*i pv. *mandevillae* (Psm) strains. **(A)** Gel electrophoresis of plasmid preparations from the indicated Psm strains. **(B)** Southern blot hybridization of the plasmids shown in **(A)** using an *iaaM* probe. M, linear DNA molecular weight marker II DIG-labelled (Roche, Mannheim, Germany); clp, chromosome and linearized plasmids. The lower hybridization band likely corresponds to chromosomal DNA and/or linearized plasmids, given their width and undefined borders, and because the genomic context of one of the two *iaaM* paralogs found in the Psm Ph3 genome contains typical chromosomally-encoded genes (contig NZ_NIAX01000097).

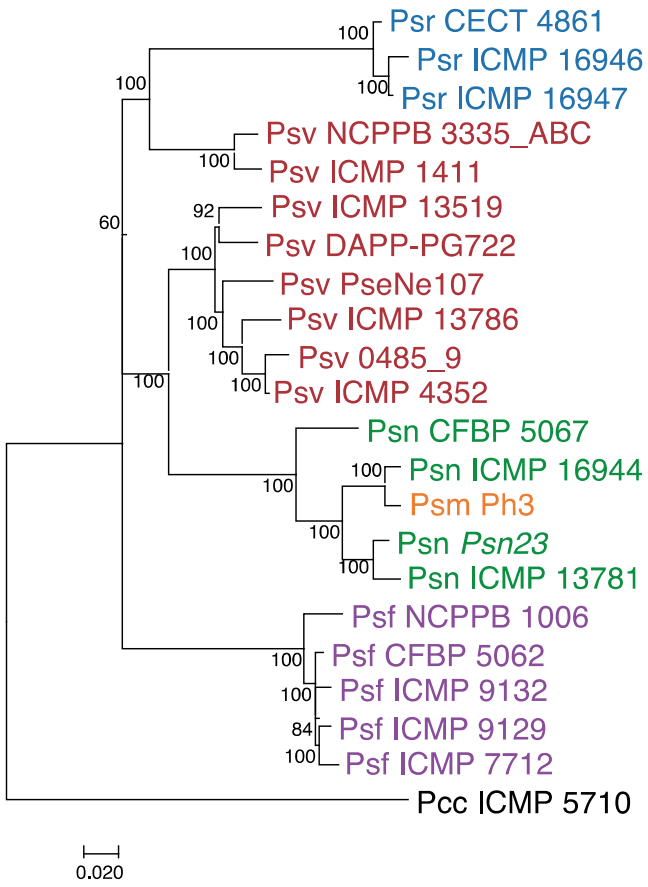

Figure S2. Maximum likelihood phylogenetic tree of *P. savastanoi* core genome SNPs. The tree was rooted with *P. syringae* pv. *ciccaronei* ICMP 5710. Values in nodes are Bootstrap percentages from 100 replicates; the scale represents substitutions per site. Psv, Psn, Psf, Psr and Psm, *P. savastanoi* pathovars *savastanoi*, *nerii*, *fraxini*, *retacarpa* and *mandevillae,* respectively. *P. savastanoi* strains are described in Table 1 or were previously described (Moreno-Pérez et al., 2020).

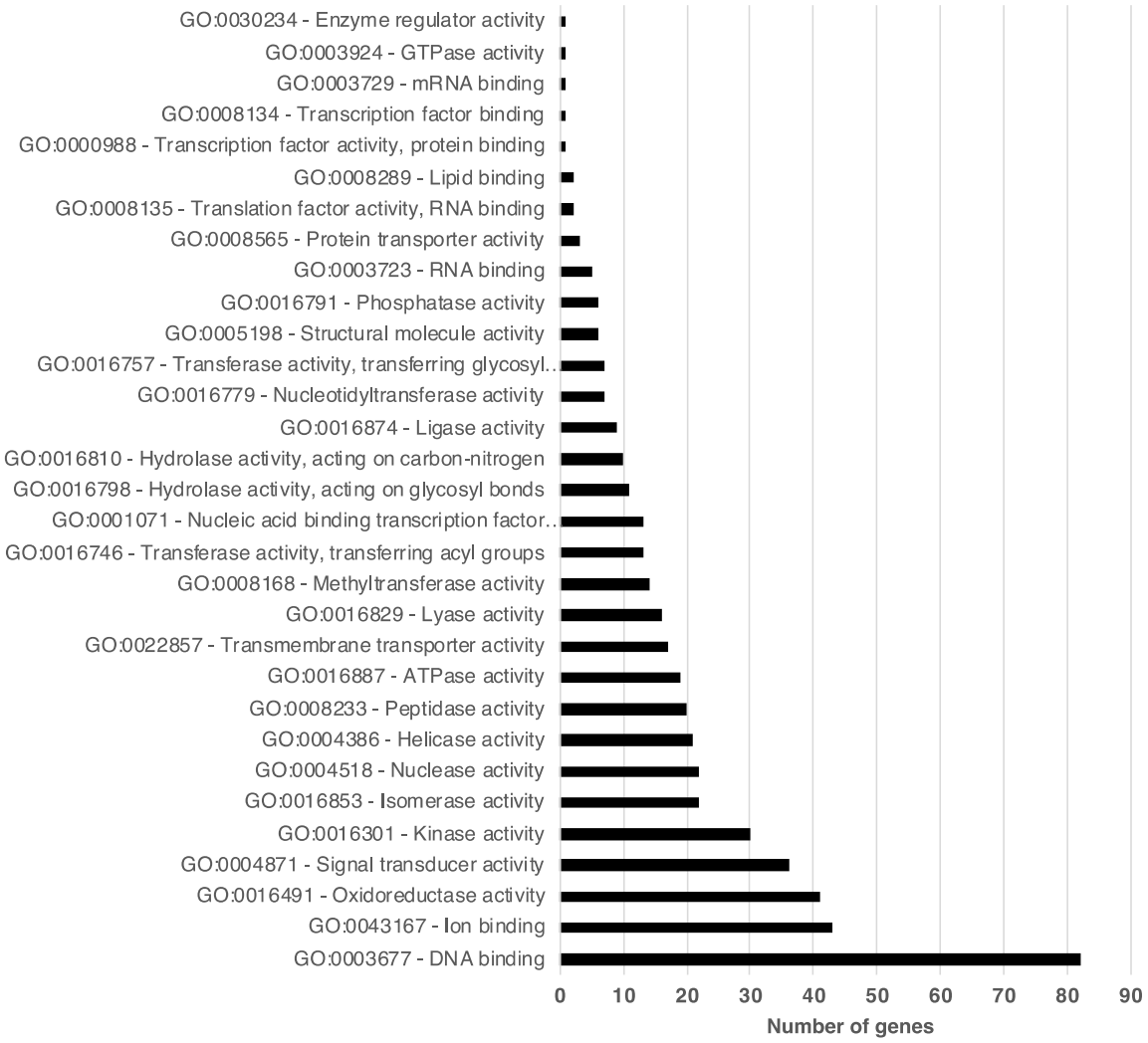

Figure S3. Predicted biological function of *P. savastanoi* pv. *mandevillae* (Psm) and *P. savastanoi* pv. *nerii (*Psn) strain-specific genes. Specific genes were classified by their predicted molecular function using Sma3s_v2 software (Casimiro-Soriguer et al., 2017).

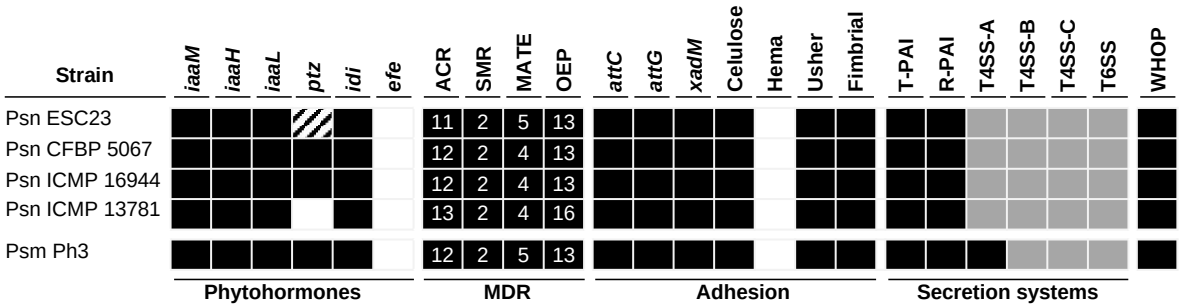

Figure S4. Bioinformatics prediction of the virulence gene repertoires of *P. savastanoi* strains using PIFAR. Black boxes and white boxes, presence or absence, respectively, of the indicated gene or gene set; asterisks, genes not found in the genome but identified by PCR; grey boxes, partial codification of core genes; striped box, a *ptz* gen (cytokinins biosynthesis) not found in the assembly but found in the unassembled reads. MDR, multidrug resistance transporter; ACR, acridine-like transporter from the resistance/nodulation/cell division (RND) family; SMR, small multidrug transporter family; MATE, multidrug and toxic compound extrusion family; OEP, outer membrane efflux protein (RND family); *attC* and *attG*, attachment gene homologs (*Agrobacterium tumefaciens*); *xadM*, adhesion gene homolog (*Xanthomonas oryzae*); Cellulose, cellulose synthase; Hema, hemagglutinin-repeat protein; Usher, outer membrane usher protein; Fimbrial, fimbrial protein. T-PAI, canonical tripartite T3SS; R-PAI, rhizobial T3SS; T4SS, type IV secretion system; T6SS, type VI secretion system. WHOP, genomic island carrying four operons and other genes involved in degradation of phenolics (Caballo-Ponce et al., 2017).

Table S1. Primers used in this study

Name	Sequence (5'→3')
gyrB_F351	GTGGTCGCGACCTTGTGC
gyrB_R920	AAGTATCCGGCGGCTTG
rpoD_F383	CGCCAAACGTATCGAAGAAG
rpoD_R1055	GCTATTTTCAGGCCGGTTTC
gapA_F220	GACCGTCAATGGTGACCG
gapA_R931	GCCCATTCGTTGTCGTACC
rpoA_F22	ATGCAGATTTCGGTAAATGAGT
rpoA_R350	GGGTTAACGATCTCGACATC
recA_F197	GATCGTGGAAATCTACGGTCC
recA_R935	GAGCGCTTTGCAGATTTCC